

THE STELLAR POPULATION OF THE GLOBULAR CLUSTER M 3

II. CCD PHOTOMETRY OF ADDITIONAL 10,000 STARS

F.R. Ferraro^{1,2}, E. Carretta^{1,2}, C.E. Corsi³, F. Fusi Pecci¹, C. Cacciari¹, R. Buonanno³, B. Paltrinieri⁴, D. Hamilton⁵

¹ Osservatorio Astronomico di Bologna, Via Zamboni 33, I-40126 Bologna, ITALY

² Visiting Astronomer, German-Spanish Astronomical Center, Calar Alto, SPAIN

³ Osservatorio Astronomico di Roma, Roma, ITALY

⁴ Dipartimento d'Astronomia, Via Zamboni 33, I40126 Bologna, ITALY

⁵ Max-Planck Institut f. Astrophysik, Heidelberg, GERMANY

Abstract. We present BVI CCD photometry for more than 10,000 stars in the innermost region ($0.3' < r < \sim 4'$) of the globular cluster M 3. When added to the previous photographic photometry by Buonanno *et al.* (1994) reaching as far as $r \sim 7'$, this results in an homogeneous data-set including about 19,000 stars measured in this cluster, which can be now regarded as one of the main templates for stellar population studies.

Our main results, from the new colour-magnitude diagrams (CMD), are:

1. Completeness has been achieved for all objects at $V \leq 18.6$ and $0.3' < r < 7'$.
2. Our new independent photometric calibration is redder than the old calibration (Sandage and Katem 1982) in the blue range, and bluer in the reddest part of the CMD. This colour term has important consequences on some issues (e.g. metallicity, period-shift effect, etc.).
3. The metallicity derived from the photometric indicators $(B - V)_{0,g}$ and $\Delta V_{1,4}$ is $[Fe/H] \sim -1.45$, i.e. significantly higher than the value -1.66 generally used so far. This is in very good agreement with the most recent high resolution spectroscopic studies of individual stars.
4. There is indication of the presence of a very faint and blue extension of the HB, although scarcely populated.
5. The population ratios of HB, RGB and AGB stars confirm the value previously found for the helium content, i.e. $Y = 0.23 \pm 0.02$.
6. There is a significant population of blue straggler stars, although the exact number must await HST data for a better resolution in the very central regions.

Key words: Galaxy: Globular Clusters: Individual: M3 - Stars: Population II - Stars: CCD photometry

1. Introduction

The advent of the charge-coupled devices technology and, very recently, the availability of the refurbished *Hubble Space Telescope (HST)*, coupled with the use of more and more sophisticated software for photometric analysis in crowded fields, have opened unique possibilities of using galactic globular clusters (GGCs) as templates for testing the stellar evolution theories (Renzini and Fusi Pecci 1988–RFP88). In particular, the combined use of both colour-magnitude diagrams (CMDs) and luminosity functions (LFs) derived from very accurate and complete photometric studies allows to reach levels of precision eventually suitable to check even the finer details predicted from updated theoretical models.

Since the basic aim is to secure stellar samples *as populous and complete as possible in any radial region* of a cluster to yield statistically significant information on all the stellar evolutionary phases (including the very short ones, $t \sim 10^4 - 10^5$ yr) and on the cluster as a whole (f.i. taking into account also the cluster internal dynamics), proper ground-based observations in the outer areas must complement *HST* observations exploiting the photometry in the very central regions.

Within this framework, we started a long-term project (ground-based + *HST*) to make M3 *one of the first and best observed templates* to verify in detail the model predictions (Buonanno *et al.* 1986, 1994, RFP88, Ferraro *et al.* 1993, Cacciari *et al.* 1993).

Why should M3 justify such a big effort? There are many good reasons. Among others, for instance: a) since the early study by Sandage (1953), M3 is one of the prototype Pop II clusters of intermediate-poor metallicity; b) it is rich of RR Lyrae variables, and is usually adopted as Oosterhoff (1939) class I prototype; c) it contains the first detected *blue straggler stars* (BSS), now suspected to have a bimodal radial distribution (Ferraro *et al.* 1993); d) its CMD displays a significant population in every branch, with an Horizontal Branch (HB) spanning a very wide range in color (temperature), including extremely blue (hot) stars and Post-Asymptotic Giant Branch objects (P-AGB); e) it has been the target of recent spectroscopic studies (including at high resolution, see for references Carretta and Gratton 1996a), yielding a new insight on its average metallicity and metallicity dispersion.

The *first* step in our project has been a wide-field survey, based on the original Sandage’s photographic plates, of regions from 2 up to 7 arcminutes from the cluster center, whose results have already been published (Buonanno *et al.* 1994–PH94). In that paper we published B, V magnitudes for more than 10,000 stars, reaching about two magnitudes fainter than the Main-Sequence turnoff (TO), with internal photometric errors mostly smaller than 0.05 mag. As a *second step*, in this paper we present the results of a new BVI CCD-photometry for almost 10,000 additional stars measured in the inner parts of the cluster. The *third* and final step to complete the survey will present the *HST* data secured on the cluster core (proposal GO 5496, P.I. F. Fusi Pecci), whose reduction is currently in progress (Fusi Pecci *et al.* 1996). A further paper specifically devoted to the BVI CCD-photometry of 65 RR Lyrae variables is in preparation (Cacciari *et al.* 1996).

In Section 2, we present the description of data acquisition and analysis, including tests for completeness and comparisons with our previous photographic results (PH94) and with other data-sets. In Section 3, we describe our results, with special emphasis on the features of the main bright branches of the CMD and, in particular, we deal with mean ridge lines, the so-called RGB-Bump, star counts, population ratios, and an update of the overall blue stragglers population in M 3. Finally, Section 4 is devoted to conclusions and schematic summary.

2. Observations, data reduction, comparisons and completeness

2.1. Observations and cluster sampling

The CCD data were obtained at the 3.6m CFHT telescope on April 1991 by H. Richer and R. Buonanno within a wider collaborative program, using a $2,048 \times 2,048$ pixels detector with field of view of $\sim 7' \times 7'$. The observations consisted of two sets of BVI frames reported in Table 1. The short exposures were specifically taken to

survey the very inner regions, avoiding strong saturation effects. Since the detector had a very poor response in the blue, Ferraro *et al.* (1993–F93) used the deepest V and I exposures to get a first hint on the BSS population in the cluster central regions ($r < 2'$).

Table 1. Observation log of the BVI CCD data

Colour	Exp.Time (sec)	Date	Seeing (arcsec)
B	120	April 7,1991	0.80
V	120	April 7,1991	0.65
I	120	April 7,1991	0.63
B	30	April 7,1991	0.85
V	10	April 7,1991	0.70
I	10	April 7,1991	0.63

Figure 1 shows the position of the area surveyed in the present study (the *full square*) overlapped to the map of the regions considered in the photographic study (PH94). For sake of clarity, the individual stars measured on the plates in the PH94 bright (*crosses*) and faint (*small dots*) sample are respectively plotted.

Fig. 1. Map of the regions of M 3 covered with the photographic survey (PH94). The *full square* reproduces the field covered by the present CCD-observations. *Crosses* indicate stars included in the PH94 *bright sample*, while *dots* indicate stars membering the photographic *faint sample*. In the map, North is up and east is to the right; the scale-unit is in arcsecond.

To give a global overview of the planned survey, we report in Figure 2 also the size and location of the three WFPC2 fields we observed with GO 5496. As it can be seen, there is a useful overlapping between the photographic, CCD, and *HST* considered areas. For comparison, we have also reported in the same figure (*dashed squares*) the fields covered by other recent photometric studies on M 3, namely those by Bolte *et al.* (1995; hereinafter BHS), Guhathakurta *et al.* (1994; hereinafter GYBS), and Burgarella *et al.* (1995) using the WFPC of *HST* before refurbishment.

2.2. Data reductions

The data analysis was performed in Bologna and Rome using ROMAFOT (Buonanno *et al.* 1979, 1983), whose standard procedures have been reported in other papers (see for references Ferraro *et al.* 1990, F93). No special re-

Fig. 2. Global overview of the fields observed in the photographic, CCD, and *HST* surveys that will compose our overall photometric data-set in M 3. The *full square* represents the contour of the CFHT field. The *dashed squares* are the fields surveyed by Bolte *et al.* (1995; label B.) and Guhathakurta *et al.* (1995; label G.), respectively. Note that the FOC-field observed by Burgarella *et al.* (1995) would be represented here by just a “central dot”. The annulus ($2.0' < r < 3.5'$; *thin solid lines*) is the region of M 3 where the “complete” sample considered in the photographic study has been obtained (PH94). The small *full circle* represents the central region (with $r < 20''$) where crowding makes unfeasible any meaningful photometry on the deep CCD-frames taken at the CFHT.

quirement has been involved either in the searching phase or in measuring the instrumental magnitudes.

Since the only wide set of standard stars available in the M3 field we observed were those measured with the photoelectric photometer by Sandage (1953, 1970), later revised by Sandage and Katem (1982), we put some effort to obtain an independent CCD-calibration. As a matter of fact, neither BHS (they only presented instrumental magnitudes) nor GYBS (who ultimately referred their magnitudes to Auriere and Cordoni 1983 and F93) obtained an independent calibration. The photometry of Auriere and Cordoni (1983) in the central regions was linked to star profiles (King 1966) and cannot be used for calibration. The data presented by Scholz and Kharchenko (1994) are referred to Sandage (1970). Finally, Paez *et al.* (1990) in their CCD-study of the outer regions (at about 5 arcmin from the cluster center) did not get any independent calibration but referred their data to 41 stars in common with Sandage and Katem (1982).

In PH94, we used the sequence of photoelectric standards from Sandage (1970) to calibrate the photographic magnitudes to the standard *B, V* Johnson system. In F93, the CFHT data were calibrated using two standard fields observed during the same nights in NGC 4147 and M 67, with the well known problems related to the difficult handling of calibrated stars in crowded standard fields. Eventually, we concluded that a new independent CCD-calibration was necessary starting from a proper set of primary standards.

After several unfruitful runs (due to bad weather, telescope failures etc.), our new calibration is based on an observing run carried out at the 1.23 m telescope at the German-Spanish Astronomical Centre, Calar Alto, Spain. BVI CCD-frames of M 3 and of several Landolt CCD standard areas were acquired under photometric conditions in the night of April 2, 1995, using a thinned 1024×1024 Tektronix chip (24μ pixels, 0.50 arcsec/pixel), with Ar-coatings. The *I* filter is in the Kron-Cousin system, centered at 8020 \AA .

The calibration of the CFHT CCD magnitudes was thus performed in two steps. First, we used 18 stars in 7

CCD standard areas (Landolt 1983) to link the Calar Alto instrumental magnitudes to the standard Johnson system. The final equations we adopted for the B,V, and I filters are reported below and plotted in Figure 3:

$$B = b + 0.215 (\pm 0.017)(b - v) + 20.386 (\pm 0.007) \quad (1)$$

$$(\sigma = 0.029),$$

$$V = v + 20.577 (\pm 0.005) \quad (2)$$

$$(\sigma = 0.020),$$

$$I = i + 20.340 (\pm 0.006) \quad (3)$$

$$(\sigma = 0.026),$$

where b,v,i, are the instrumental magnitudes.¹ The atmospheric extinction terms in each colour have been derived by observing the same standard field at different airmass during the night.

Fig. 3. Calibrating Landolt CCD standard stars used to transform the instrumental Calar Alto magnitudes to the Johnson standard system. Different symbols refer to stars in different standard areas.

In the *I* calibration we have used only the measurements having a sufficient S/N. In particular, this has led to exclude two of the bluest standard. because of this, we could exclude the existence of residual colour terms for the *I* band.

These equations have been used to calibrate the instrumental magnitude of a sample of ~ 100 isolated, unsaturated stars in the Calar Alto frames for which the aperture photometry has been performed. This set of stars has been used to correct the CFHT magnitudes (previously calibrated with the NGC 4147 and M 67 standard fields, see F93). The relations linking the “old” CFHT calibration system to the new standard system (CCD96) are:

$$V_{\text{CCD96}} = V_{\text{CFHT}} + 0.02(B - V)_{\text{CFHT}} - 0.004 \quad (4)$$

$$B_{\text{CCD96}} = B_{\text{CFHT}} + 0.03(B - V)_{\text{CFHT}} - 0.006 \quad (5)$$

$$I_{\text{CCD96}} = I_{\text{CFHT}} - 0.03(V - I)_{\text{CFHT}} + 0.054 \quad (6)$$

Following the above procedure we linked the whole CFHT-CCD data set to the Johnson system. In the next section we find the relation to transform the photographic data set to the new standard system here adopted.

¹ Throughout this paper, the symbol σ will indicate the standard deviation of a single measurement, while the value after the symbol \pm will refer to the standard deviation of the mean.

In this respect, it is important to note that, after completion of our reductions, we became aware of the existence of a new independent photometric study of a very wide sample of M3 stars (about 23,700) carried out by K.A. Montgomery (1995 – M95) as part of his Ph.D. dissertation, based on 2048×2048 (T2ka) CCD-frames taken with the 0.9-meter telescope at KPNO. Since with the f/7.5 secondary, the telescope produced an image scale of 0.68 arcsecs/px and a field of view of 23.2 arcminutes, and moreover 2×2 mosaics of images were made with the centers offset by 10 arcminutes in both right ascension and declination, the total field covered by Montgomery fully overlaps both our field and the outer field independently observed by Stetson and Harris (1988), which being located outside the region we observed could not be used in our photometry. We will discuss in detail the results of the comparisons with this new data-set at Sect. 2.4 and 2.5.

2.3. Photographic vs. CCD photometry; magnitudes and positions for the global sample of M 3

More than 900 stars have been found in common between the CCD96 and PH94 (bright and faint) sample. However, due to the limited performances of the used CCD detector in the blue band, the photometric internal errors in the B band are large and reduce the reliability of the transformations. For this reason only 532 bright ($B < 18.6$) stars in common have been used to derive the relations linking the photographic photometric system to the standard system here adopted. The final relations correcting the V magnitude and the $B - V$ colours are:

$$V_{\text{CCD96}} = V_{\text{PH94}} + 0.08(B - V)_{\text{PH94}} + 0.053 \quad (7)$$

$$(B - V)_{\text{CCD96}} = (B - V)_{\text{PH94}} - 0.143(B - V)_{\text{PH94}} + 0.096 \quad (8)$$

These corrections have been applied to the whole (bright + faint) PH94 sample. A small residual non-linearity in the photographic data (probably due to the original plate transformation) has been corrected using a polynomial fit of 5th order (to yield C_V^{5th} and C_B^{5th} for the V and B filter, respectively). This additional correction is properly determined only for bright stars ($B < 16.8$, $V \sim 17.8$).

Resting on our own data alone, it would be impossible to check properly the linearity of the fainter PH94 measures. However, by comparing our data with the quite similar data-set obtained by M95, we can extend the linearity test to fainter magnitudes, as explained in Sect. 2.4. From this last comparison we have obtained further (small) corrections for the fainter stars (see Sect. 2.4) using a similar procedure as adopted for the bright sample.

Then, to avoid any discontinuity at the junction between the bright and the faint PH94 samples, we have imposed coincidence between the corrections computed at

the junction [C_V^{5th} and C_B^{5th}] from the two different CCD data-sets. Fortunately, they actually turned out to be almost equal, and this reinforces both the validity of the procedure and the achievement of a good linearity all over the “revised” PH94 sample.

In Figure 4 and Figure 5, we present the ($V, B - V$) and ($V, V - I$) CMDs containing only stars outside a radius of 20” from the cluster centre, excluding the variables which are however included in the lists. Due to the low efficiency in the blue of the CFHT CCD-camera we have plotted in Figure 4 only the objects measured on our B CCD images with $B < 18.6$. In particular, the upper part of the $V, B - V$ CMD (brighter than $B = 18.6$) contains 2227 constant and 154 variable stars taken from the CFHT CCD sample, plus 42 variable stars and 444 constant stars taken from the *bright* photographic sample outside the CCD field. For magnitudes fainter than $B = 18.6$, we report the 9339 stars from the *faint* PH94 sample. The total number of stars in this CMD is therefore 12206. The $V, V - I$ colour magnitude diagram contains 9647 stars including 155 variables that have both V and I magnitudes.

Fig. 4. CCD96 $V, B - V$ colour-magnitude diagram for 12206 stars in M 3 with $r > 20''$. Variable stars are not shown; only stars with $B < 18.6$ from the CFHT sample have been plotted. See text for details.

Fig. 5. CCD96 $V, V - I$ colour-magnitude diagram for 9647 stars in M 3 with $r > 20''$. Variable stars are not included in the plot, see text for details.

All the available data (magnitudes and positions) are available upon request from the authors, and will also be sent to Strasbourg Data Center. As in the PH94 paper, X, Y coordinates (in arcsec) are referred to the cluster centre, taken at $\alpha_{1950} = 13^h 39^m 24^s$ and $\delta_{1950} = +28^{\circ} 38'$. Coordinate transformation to other systems can be easily performed; to help with cross-identification, we note that our bright stars No. 8877, 10052 and 12045 are the stars No. 9, 3842 and 2267, respectively, in the photometric catalogue of GYBS. This allows conversion of our positions to equinox 2000 coordinates, since GYBS’s positions are in R.A. and Dec. referred to the equinox 2000.

2.4. Comparison with other studies

We compare here our CCD-calibrated photometry with the data taken from other studies for the stars in common.

• Comparison with Sandage and Katem 1982

The comparison was made using 81 stars from Tables I and II of SK82, cross-identified with our data. The results

of this comparison, together with the least squares fits through the data, are shown in Figure 6.

As one can see, the overall agreement is good, but there are also important differences. First, there is a luminosity shift in both B and V, variable with varying the B-V colour. Second, there is a quite noticeable colour term, in the sense that our data are ~ 0.08 mag redder at $B - V = -0.2$ (the bluest point of the HB), ~ 0.03 mag redder at $B - V = +0.3$ (corresponding to the middle of the instability strip), and ~ 0.08 mag *bluer* at $B - V = 1.6$, *i.e.* at the termination of the Red Giant Branch (RGB).

Fig. 6. Differences between our calibrated magnitudes and those from Sandage and Katem (1982) for 81 stars (extracted from his Tables I and II). In each panel the equations of the least-squares fits (solid lines) to the data are also reported.

- *Comparison with Guhathakurta et al. 1995*

Figure 7 shows the results of a similar comparison with the V and I magnitudes of GYBS for 634 stars, almost down to the completeness limit of the survey. GYBS studied the central field of M 3 using the F555W and F785LP bands of the *HST/Planetary Camera-1*, that are similar to the Johnson V and I bandpasses, respectively.

As explained below, this comparison is actually more useful for checking completeness since, after a first colour transformation from *HST* instrumental magnitudes, GYBS linked their photometry to the available ground-based data. In particular, their final values include the application of zero-point offsets to the V and I data to match fiducial points of the upper parts of the CMDs presented by Auriere and Cordoni (1983) and F93. The generally good agreement shown Figure 7 is thus obvious though the F93 CCD calibration was still based on the NGC 4147 and M67 standard areas.

Fig. 7. Residuals between CCD96 V and I magnitudes and the corresponding photometry of GYBS in the F555W (V) and F785LP (I) bands of *HST/Planetary Camera-1* (see text). The comparison is based on 634 stars in common within the area covered by GYBS.

- *Comparison with Montgomery 1995, and Stetson and Harris 1988*

Concerning the data-set obtained by M95, we present here the results of the comparisons made using the still preliminary list of magnitudes and colors kindly made available to us by Dr. K. Janes. Since they could still be subject to further analysis and revisions, and will be eventually published in the near future (Janes and Montgomery, 1996), we schematically report on two main aspects which are of

interest for the present study: the linearity test and the comparison of the zero-points.

Concerning the linearity test, after carrying out several different procedures, we decided to restrict the sample to a sub-set of the 7,152 stars in common (from the RGB tip down to the faintest magnitude limit), which have unambiguous identifications, no detected companions in both photometries, and sufficiently low and well defined background. This implies that these stars lie mostly in the outer cluster regions and have good internal photometry in both studies.

From the study of the residuals it is confirmed that, while no significant trend is evident after the corrections applied to the bright PH94 stars using our corresponding CCD data (see Sect. 2.3), there is still a small residual non-linearity in the faint photographic PH94 data, quite similar in size and morphology to that detected for the bright stars with respect to our CCD measures. Therefore, we have corrected the faint PH94 measures using again a polynomial fit of 5th order (computed over $\sim 3,800$ faint stars) as done for the bright stars, and imposing coincidence of the (small, ~ 0.01 - 0.02 mag) linearity corrections at the junction between the bright and faint samples (see Sect. 2.3).

The comparison of the zero-points has also been made on a special sub-set of about 2,000 stars, chosen within the sample considered for the linearity test but with $V < 19.5$ (to avoid low S/N data). The final figures for the differences, in the sense *M95 - Ours*, are: $\Delta V = -0.06$, $\Delta B = -0.11$, $\Delta B - V = -0.05$ mag, respectively. As can be seen, especially for the B-magnitudes, the residuals are quite large and somewhat worrying.

Based on the description reported in Table 2.1 and Fig. 2.3 of his thesis, Montgomery observed Standard Star fields from Landolt (1992) over the six night run at KPNO, securing approximately 250 measurements with internal accuracy in the individual measure better than 0.05 mag. The KPNO run standard deviations of the residuals he quoted were 0.018 in V and 0.024 mag in B, quite comparable with the figures from our own calibration (see eqs. (1)-(2)). It is therefore difficult to explain the differences between the zero-points adopted in the two photometries based just on the formal errors. And it is also difficult to choose which of the two may be correct. To have further insight on this important aspect, we have carried out a further comparison with the data obtained by Stetson and Harris (1988, -SH88).

Since there is no overlap by SH88, we must use the comparisons (for different sets of stars) between M95 and SH88 on the one hand, and M95 and this study, on the other, to provide a link between SH88 and our photometry. So doing, we get that the differences between our data and SH88 (in the sense *Ours - SH88*) are: $\Delta V = +0.04$, $\Delta B = +0.04$, and $\Delta B - V = 0.00$ mag. These figures are compatible with the residuals measured by Montgomery

with respect to SH88. From Fig. 2.13 and Table 2.3 of Montgomery (1995) one has in fact for the residuals $M95 - SH88 \Delta V = -0.048$, $\Delta(B - V) = -0.020$ mag, based on 27 stars in common with SH88. As a matter of fact, the zero-points of SH88 turn out to be intermediate between the other two photometric calibrations.

2.5. Error estimates and choice of the zero-points

Since we have only two frames in each colour with quite different exposure times, we cannot use repeated measures of the same star to yield a direct estimate of the *internal* measuring errors. However, we can get some quantitative hints from the photometric parameters listed for each star within ROMAFOT (which essentially trace the quality of the fit) and from the comparison of the morphology of the individual branches in the CMD (at different magnitude levels) with those obtained in previous studies. In particular, using also as reference the error estimates discussed in PH94, we are fairly confident that the *internal* errors in the present photometry are ~ 0.02 – 0.03 mag at $V < 18$, and ~ 0.05 at the TO region.

Concerning the *systematic* errors, we have already discussed the problems related to the zero-points and the colour transformations. There are now three independent calibrations referred to observations of Landolt’s (1992) standards. They are in marginal agreement, but it is difficult at the present stage to choose which is the best.

Since the calibration here adopted seems to be compatible with that obtained by Stetson and Harris (1988) (they actually show a systematic difference of 0.04 both in B and V, yielding however no colour difference), we decided to keep using our calibration.

To be conservative and taking into account the size of the uncertainties, we conclude however that we still cannot exclude errors as high as 0.05 mag in the *absolute* values, both in magnitude and in colour (particularly at the blue and red extremes).

Such a conclusion is quite disappointing in particular for what concerns the specific study of the RR Lyrae variables (Cacciari *et al.* 1996), and further efforts to improve the absolute calibrations are urged.

2.6. Completeness of the CMDs

Besides the comparisons in colour and magnitude discussed above, the BHS, GYBS, and M95 samples can be also used to test in a quantitative way the degree of completeness actually achieved in the present photometric data set. These checks can be performed on different subsets, depending on the regions and the magnitude range covered in the different studies.

• Comparison with Bolte *et al.* 1993

Of particular interest is the comparison with the BHS’s samples, since they were obtained with the same CFHT telescope, “under apparently photometric conditions and

with excellent seeing”. A careful check is feasible using all stars brighter than $V = 16.75$, the limit in V used by BHS for the reference population in order to study the blue stragglers distribution (see below). The result of this check is plotted in Figure 8 that compares the $(V, V - I)$ CMD we have obtained from surveying the same area as BHS (see Figure 2) with their $(V, V - R)$ diagram. Note that their instrumental V magnitudes have been transformed to our system by using the brightest ($12.5 < V < 17.0$) 544 stars in common.

Fig. 8. Comparison of the upper part of our CMD (panel b) with that of BHS (panel a) in the region covered by their study, for stars brighter than $V = 16.75$. Instrumental v magnitudes of BHS have been shifted to match our own calibrated V system. Variable stars are here included and this explains the “fatness” of the HB (see text).

In the region in common between the two samples, BHS have found 801 stars while we detected 831 objects, at $V < 16.75$. Among these, 775 stars were successfully cross-identified, whereas 26 stars from BHS and 53 stars from our survey had no mutual correspondence. However, we must note that most of these residual stars lie on the faint RGB, just above the threshold ($V = 16.75$) adopted to carry out the comparison. Therefore, the difference in the samples essentially depends on small variations in the arbitrary offset necessary to match the two data-sets in V and on photometric errors. Since the stars plotted in the CMD of Figure 8 are the same and the observing conditions of the BHS run were excellent, the overall appearance of the two CMDs confirms also the good *internal* quality of our photometry. Note that the width of the red HB (in particular) is due to the inclusion of randomly phased measures of the variable stars.

• Comparison with Guhathakurta *et al.* 1995

A similar check has been carried out with the GYBS data. Figure 9 presents the CMDs for the stars independently detected and measured in the common area covered by the two studies (see Figure 2, $r \simeq 1'$). In this region, we have found 340 stars while GYBS list 339 objects. Of them, 15 and 16 stars in the GYBS and in our subsamples, respectively, do not have cross-identification. As for BHS, they mostly lie near the faint limit of the selected subsets, and the difference is thus due to the selection bias induced by the photometric scatter.

By inspecting Figure 9, it is also interesting to note the difference in photometric quality achieved in the two samples. Since the GYBS data have been obtained using the *HST* WFPC1, the larger internal scatter is most likely due to the difficulty of measuring “aberrated” stars in the inner crowded region. On the other hand, the excellent agreement in the total numbers of selected objects confirms the very high degree of completeness achieved in

our ground-based survey (note that the searching phase is almost “perfect” for the bright objects also with *HST* WFPC1).

Fig. 9. Comparison of the upper part of the CMD by GYBS (panel a) with our data (panel b) in the spatial region in common to both studies. The dashed line reports the Horizontal Branch and bright Red Giant and Asymptotic Branch limit as adopted in Figure 7 of GYBS.

The comparisons discussed above can be considered as *external* independent checks of the degree of completeness actually achieved in our searching phase, at least as far as the upper part of the CMD is concerned. The results of the comparison have shown that completeness is close to 100% even using the *HST* sample as reference. Since this comparison refers to the innermost regions of the cluster, where completeness is most problematic, we are confident that a similar very high degree of efficiency has been guaranteed by our searching routine in the more external fields. Additional tests made adopting the usual “artificial star” procedure fully confirm this conclusion.

- *Comparison with Montgomery, 1995: the bright sample*
The availability of the new catalog compiled by Montgomery (1995) has offered the opportunity to carry out a preliminary check of completeness all over our observed field as his observations fully overlap our considered regions. Since the limiting magnitudes of the two surveys vary with the cluster regions, we have separated the analysis of the bright sample from that of the faint one.

Fig. 10. Comparison of the upper part of the CMD by M95 (panel a) with our data (panel b) in the spatial region in common to both studies. Only stars with $B < 18.6$ have been plotted. Variable stars are here included.

Figure 10 shows the CMDs obtained from the two photometries down to $B = 18.6$, considering just the overlapping area. As can be seen, apart from a slightly larger scatter in M95 data, the overall morphology is very similar and also the total number of stars is comparable. This evidence by itself confirms that the degree of completeness achieved in the two studies is also similar and high. We have detected 2841 stars while M95 lists 2750 objects. However, to have quantitative hints of the completeness of our sample it is useful to check the number and properties of the objects which are present only in the M95 sample, as they could have been missed in our search.

Figure 11 shows the CMD (*panel a*) and the map (*panel b*) of the objects M95 detected on our field and we apparently missed. It is quite evident that they are mostly located in the very central regions where the resolving ca-

Fig. 11. $V, B - V$ CMD (panel a) and map (panel b) of the stars detected by M95 on our area and not cross-identified with objects detected by ourselves. Coordinates are in arcsec with respect to the cluster center (see Section 2.3).

pability of the two surveys is different, our own being much better. A careful interactive analysis of a subset of these objects has shown that most of them are actually blended images which we resolved into two (or more) separated stars with off-center positions with respect to the blend. If we increase the size of the box (from 0.5 to 1.0 arcseconds) we get multiple identifications with the individual components.

The few bright stars located at the outskirts of the considered field are lacking in our samples as they are “field” stars according to Cudworth (1979) or because they are highly saturated standards.

To summarize the comparisons and to give a further insight on the mutual completeness of the four considered samples, we have plotted in Figure 12 the ratios between the number of stars measured by BHS (*panel a*), GYBS (*panel b*), and M95 (*panel c*), respectively, and the number of stars we measured per bin of 0.5 mag in V . The comparison is obviously made on the areas in common between each quoted study and our own survey. Error bars have been computed by simply taking the inverse of the square of the total number of stars in each bin. As can be seen the bright samples are substantially the same especially considering the effect of binning over CMDs which have slightly different calibrations and local morphologies.

In conclusion, based on the tests here carried out and on those already reported for the outer samples considered in PH94, we can say that most likely all the objects brighter than $V = 16.75$ have now been detected and measured in a circular annulus with $0.3' < r < 7'$ in M3.

Fig. 12. Comparison of the number of stars we included in the bright samples with the corresponding lists by BHS (panel a), GYBS (panel b) and M95 (panel c). The ratios of the numbers of stars we found to those measured by BHS, GYBS, and M95, respectively, are presented over 0.5 mag bins in V .

- *Preliminary comparison with our own HST-data: the bright sample*

The considerations made above are sufficient to assess the degree of completeness necessary in determining the populations of the bright RGB and AGB (down to ~ 1 mag below the HB). However, further discussion is required concerning the completeness of the faint, blue HB tail which plays a rôle in the computation of the various population ratios we are going to discuss later.

Since we have specifically taken deep UV exposures with *HST* to study this aspect and a detailed paper is

in preparation, we simply anticipate here the essence of the results. The preliminary reductions of the *HST* data confirm that there is no significant population in the HB blue tail fainter than $V \sim 17$ (for $r > 20''$) except for the objects we have detected with the present BVI CCD-survey and the old PH94 study.

In particular, in the area in common between the present sample and the *HST* survey, we have detected 8 objects in the CCD frames lying at $B - V < 0.1$, $17.0 < V < 18.5$ and 8 objects in the *HST* frames. Although the detected population is small and the membership to the HB blue tail is somewhat uncertain given the photometric scatter, this ensures that the loss of candidate faint HB stars should be small and in any case quite negligible in the computation of the global population ratios (see Sect. 3.5).

Outside $r > 110''$, where HST-data are not available at present, we rest on the tests for completeness carried out on the photographic plates used in PH94. On the other hand, with decreasing significantly the degree of crowding, the degree of completeness raises quite steeply.

In conclusion, from the available data there is no evidence that the stellar counts of the HB (down to $B = 18.6$, with $B - V < 0.1$) and the AGB and RGB (down to $V = 16.75$) are affected at any significant level from incompleteness. Hereinafter, we will refer to this subset as the **Bright Complete Sample (BCS)** to be used for computing useful population ratios (see Sect. 3.5).

- *Comparison with Montgomery, 1995: the global sample over the annulus with $3.5 < r < 6.0$ arcmin*

In PH94 we presented a CMD including all the stars we measured within the annulus with $3.5 < r < 6.0$ arcmin. The degree of completeness of that sample was checked using various techniques, but it was impossible at that time to make any comparison with similar observations in the same field. We have now the opportunity to directly compare our data with the M95 sample over the same annulus and get some useful information.

Fig. 13. Comparison of the upper part of the CMD using data from M95 (panel a) and from the present work (panel b). This comparison is limited to the annulus between $r = 3.5$ and $r = 6$ arcmin.

Figure 13 presents the CMDs for the objects measured in the two surveys in the considered annulus. As already noticed for the bright samples, they are very similar and consistent. Of course, the total numbers of measured objects are different mostly because the limiting magnitude we reached is deeper.

To make a quantitative comparison it is therefore useful to compute the population ratios over magnitude bins large enough to avoid small number fluctuations. Figure 14 shows the distribution of the observed ratios as

a function of the V magnitudes. As can be seen, down to $V \sim 18.5$ the two samples are essentially identical and, presumably, “truly” complete. For fainter magnitudes, our own sample clearly outnumbers the M95 list.

Fig. 14. Ratios of the stars detected by M95 and in the present work over the completeness annulus ($3.5 < r < 6$ arcmin) defined above. Data are binned in 0.5 mag bins in V .

In conclusion, this comparison adds further confirmation that the samples we secured on the various regions of M3 we observed are sufficiently complete to be used for testing the evolutionary models.

3. Results

Figure 15 and Figure 16 present our CMDs in different radial annuli, and clearly show how the different (CCD and photographic) sub-samples have been joined, as well as the main features of the individual branches. Since the lower part of the V , $B - V$ colour-magnitude diagram (composed only by re-calibrated photographic data) was discussed at length in PH94, we will concentrate here exclusively on the bright part of these CMDs.

Fig. 15. V , $B - V$ CMD at different radial distances.

Fig. 16. V , $V - I$ CMD at different radial distances.

The main aspects worth of note are the following:

1. The main branches can easily be delineated in any radial bin, including the most internal region. In particular, the RGB and the AGB can be separated quite easily at the AGB base, located at $V \sim 14.9$. The Giant Branch can easily be traced up to the tip, which is located at $V = 12.63$, $B - V = 1.58$ (star # 4191). The RGB-bump is also clearly detectable as a clump of stars at $V \sim 15.45$ (see below).
2. Despite the increased scatter in the CCD sample due to crowding in the inner regions (and to the bright plate limit in the B CFHT-exposures just above $B = 18.6$), the matching of the different samples is adequately smooth. The bulk of stars located just above the TO-region within the colour range $0. < B - V < 0.65$ are most probably the result of *optical blending* of two bright MS-stars of similar colour yielding a blend approximately 0.75 mag brighter than the individual components. This conjecture is further supported by their progressive disappearance with distance from

the crowded central regions. The difficulty of properly separating these objects represents a crucial problem in the study of the Luminosity Function of the SGB. As already discussed for instance by Ferraro *et al.* (1992a,b), some of these stars may also be blends of SGB objects and blue stragglers.

3. The HB is narrow and, over the considered region ($0.3' < r < 7'$), it contains 186 variable stars, which have not been plotted in Figure 15 and Figure 16. The blue HB tail extends down to $V \sim 18.6$, about half a magnitude brighter than the TO-level, and there is little doubt that this extremely blue HB population is quite clearly detached from the bulk of the other HB stars by a discontinuity in the population at $V \sim 16.8$ – 16.9 (see also Section 3.3 in PH94). There are also a few stars about half a magnitude brighter than the average luminosity of the HB, $\langle V_{\text{HB}} \rangle$, and located within $2'$ from the cluster center. While the possibility of field interlopers seems quite improbable given the high galactic latitude of the cluster, their presence could be due to “optical blending” between HB and RGB components or to the existence of a more evolved (*supra*–HB) population.
4. Several candidate blue stragglers have been detected and discussed in F93. Their distribution is better seen in the V , $V - I$ CMDs, where they trace, as expected, a continuation of the Main Sequence.

3.1. Mean ridge lines for M 3

Normal points for the main branches in the CMD of M 3 (MS, SGB, RGB, HB and AGB) are presented in Table 2. As usual, mean ridge lines for each evolutionary phase have been derived by plotting magnitude and colour histograms along each branch and by rejecting the most deviating objects via a $k\sigma$ – *clipping*.

Specifically concerning the determination of V_{HB} , we have computed a running mean over a 0.2 mag box moving along the HB in colour; this procedure yields a value $V_{\text{HB}} = 15.66 \pm 0.03$ which represents the average magnitude level of the HB, thus including the effects due to evolution off the Zero Age HB (ZAHB) within the instability strip.

This value is the mean level of the HB obtained from the constant stars (at the edges of the instability strip). The mean magnitudes of the RR Lyrae variables within the strip will be discussed elsewhere. The associated uncertainty is the observed *rms* vertical scatter of the HB at that colour.

Although evolution off the ZAHB is short compared to the lifetime of the ZAHB-phase (i.e. that spent at almost constant luminosity, see f.i. Sweigart and Gross 1976, Sweigart *et al.* 1987, Lee *et al.* 1990), one should quite carefully distinguish between the *average* HB luminosity and the ZAHB luminosity. There are essentially two ways to take this difference into account: the first, by adding a small positive correction to V_{HB} ($\sim 0.03 - 0.05$ mag)

Table 2. Mean ridge lines

RGB+SGB+MS V	B-V	RGB V-I	HB V	B-V	AGB V	B-V
12.50	1.648	1.706	15.11	0.684	15.06	0.694
12.70	1.509	1.554	15.18	0.671	14.87	0.733
12.90	1.371	1.441	15.25	0.660	14.70	0.771
13.10	1.280	1.370	15.40	0.617	14.52	0.801
13.30	1.208	1.311	15.56	0.573	14.38	0.831
13.50	1.131	1.249	15.61	0.534	14.23	0.863
13.70	1.067	1.206	15.67	0.450	14.08	0.904
13.90	1.019	1.169	15.67	0.400	13.93	0.939
14.10	0.982	1.135	15.67	0.350	13.78	0.978
14.30	0.949	1.106	15.67	0.300	13.62	1.027
14.50	0.919	1.076	15.67	0.250	13.46	1.084
14.70	0.890	1.053	15.68	0.200	13.28	1.154
14.90	0.863	1.032	15.68	0.178	13.08	1.239
15.10	0.840	1.009	15.70	0.158		
15.30	0.820	0.984	15.72	0.144		
15.50	0.803	0.963	15.75	0.129		
15.70	0.789	0.948	15.80	0.110		
15.90	0.770	0.932	15.86	0.092		
16.10	0.768	0.913	15.92	0.073		
16.30	0.757	0.899	15.96	0.064		
16.50	0.744	0.886	16.00	0.057		
16.70	0.733	0.869	16.26	0.020		
16.90	0.722	0.858	16.53	-0.023		
17.10	0.712	0.850	16.79	-0.060		
17.30	0.702	0.838	16.94	-0.072		
17.50	0.692		17.14	-0.093		
17.70	0.682		17.50	-0.123		
17.90	0.669		17.88	-0.153		
18.10	0.648		18.23	-0.183		
18.30	0.627					
18.50	0.534					
18.70	0.477					
18.90	0.450					
19.10	0.443					
19.30	0.448					
19.50	0.460					
19.70	0.471					
19.90	0.484					
20.10	0.503					
20.30	0.525					
20.50	0.549					
20.70	0.573					
20.90	0.598					
21.10	0.629					
21.30	0.664					
21.50	0.700					
21.70	0.737					
21.90	0.773					

to compensate for evolution; the second, by adopting as V_{ZAHB} the *lower* envelope of the HB distribution in luminosity within the instability strip (corresponding at $\text{Log } T_e \sim 3.85$). Using our HB sample, we would get $V_{\text{ZAHB}} = 15.70$ in both approaches.

Since all these effects are actually partially smeared out by the photometric errors, the difference between the ZAHB and the average levels is only marginally significant. In conclusion, we will adopt $V_{\text{HB}} = 15.66 \pm 0.03$ and $V_{\text{ZAHB}} = 15.70 \pm 0.03$.

3.2. The metallicity of M 3: a major change?

Based on the results presented in the previous Sections, we can now derive a new estimate of the metal abundance of M 3 using the so-called *photometric* indicators.

The main photometric parameters related to the cluster mean metallicity are $(B - V)_{o,g}$ (Sandage and Smith 1966) and $\Delta V_{1.4}$ (Sandage and Wallerstein 1960). Adopting $V_{\text{ZAHB}} = 15.70$, $E(B - V) = 0.00$ (see Table 10 of PH94), and the mean ridge line of the RGB listed in Table 2, we obtain $(B - V)_{o,g} = 0.80 \pm 0.03$ and $\Delta V_{1.4} = 2.81 \pm 0.03$. Using then the relationships quoted in Table 3 we derive values for $[\text{Fe}/\text{H}]$ ranging from -1.68 to -1.45 dex.

Table 3. Metallicity of M 3 from the RGB photometric parameters

Calibration	References	$[\text{Fe}/\text{H}]$
$4.30[B - V]_{o,g} - 5.00$	Zinn & West 1984	-1.56
$3.84[B - V]_{o,g} - 4.63$	Gratton 1987	-1.56
$4.68[B - V]_{o,g} - 5.19$	Costar & Smith 1988	-1.45
$2.85[B - V]_{o,g} - 3.76$	Gratton & Ortolani 1989	-1.48
$-0.924\Delta V_{1.4} + 0.913$	Zinn & West 1984	-1.68
$-1.01\Delta V_{1.4} + 1.30$	Costar & Smith 1988	-1.54
$-0.65\Delta V_{1.4} + 0.28$	Gratton & Ortolani 1989	-1.54

Another *photometric* estimate of the metal abundance of M 3 can be obtained from the CMD in the $(V, V - I)$ -plane by exploiting the iterative method recently defined by Sarajedini (1994). From the mean ridge line listed in Table 2, we obtain $(V - I)_{o,g} = 0.951$, $\Delta V_{1.2} = 1.82 \pm 0.14$, $E(V - I) = 0.00 \pm 0.05$, and, eventually, $[\text{Fe}/\text{H}] = -1.45$ with a formal error of ± 0.17 dex.

From Table 3, the lowest metallicity value is the same as the widely used figure from Zinn and West (1984; $[\text{Fe}/\text{H}] = -1.66$), and is based on their metallicity-scale calibration obtained via integrated cluster observations.

The higher value (-1.45) is based on direct spectroscopic determinations of $[\text{Fe}/\text{H}]$ from individual stars, as opposed to the integrated indexes used by Zinn and collaborators. The latest high resolution spectroscopic investigations, namely Sneden *et al.* (1992; SKPL) and Carretta and Gratton (1996a; CG96), show that the problem of the reliable measure of the metal abundance of this template cluster is not trivial at all.

In fact, SKPL found $[\text{Fe}/\text{H}] = -1.46$ from the analysis of 7 stars (and a slight different value of -1.42 by adding 3 other stars, see Kraft *et al.* 1995), and CG96 derived $[\text{Fe}/\text{H}] = -1.34 \pm 0.02$ ($\sigma = 0.06$) from 10 stars. Both studies are based on high resolution, high signal-to-noise CCD echelle spectra of high quality. In particular CG96 have re-analysed the equivalent widths published by SKPL for M 3 and other clusters to obtain a new, homogeneous metallicity scale for 24 calibrating clusters.

The main differences between the two quoted studies (apart from minor changes in the adopted values for the microturbulent velocity) are in the set of adopted atomic parameters (in particular oscillator strengths *gf* for Fe I and Fe II) and in the choice of the model atmospheres used in the analysis. CG96 used the latest, updated models from the grid of Kurucz (1992), that allow an homogeneous comparison between solar and stellar abundances, alleviating a major drawback of any former analysis of abundances for globular cluster stars.

In fact, as discussed by CG96, all previous spectroscopic determinations of the $[\text{Fe}/\text{H}]$ content of globular cluster stars were actually systematically uncertain because of the large differences (~ 0.15 dex) still existing in the reference solar value adopted in the absolute analyses. In particular, a significant discrepancy persists in the solar Fe abundances as obtained using the Holweger and Müller (1974-HM) semi-empirical solar model (usually considered to be the best reproduction of the solar atmosphere) and the model atmospheres proposed by Bell *et al.* (1976), generally adopted (also in the SKPL papers) in the analysis of cool cluster giants (see also Leep *et al.* 1987). The crucial problem thus is to find a firm answer to the question: *what is the correct solar abundance to adopt as reference for Fe?*

The recent analysis by CG96 has apparently settled the discrepancy as they have obtained a revised determination of the solar Fe abundance which is very similar to the value given by the HM model. This result has been obtained by using the set of *gf* values discussed in CG96 and a solar model extracted from the same grid of Kurucz (1992) models as used for the analysis of the cluster giants. Consequently, the study of CG96 yields a systematic difference, $\Delta[\text{Fe}/\text{H}] = +0.12 \pm 0.01$ ($\sigma = 0.08$ over 162 stars analyzed; 0.08 in the case of M 3) with respect to previous analyses, which used the Bell *et al.* (1976) models that are ~ 150 K cooler than HM in the line formation region. Therefore, even if the observational material (*i.e.*

the equivalent widths) is the same, the analysis of CG96 seems to be more self-consistent than that of SKPL.

Since the precise determination of the metallicity of M 3 has important implications on various items (f.i. on the long-standing problem of the so-called Sandage Period Shift Effect, see Sandage 1993), it may be useful to analyse further the discrepancy between the value $[\text{Fe}/\text{H}] = -1.66$ obtained via the Zinn and West (1984) calibration and the significantly higher $[\text{Fe}/\text{H}] \sim -1.4$ obtained from high-resolution spectroscopy.

Zinn and West (1984) based their estimates on integrated cluster features ultimately calibrated using old (and sometimes uncertain) $[\text{Fe}/\text{H}]$ abundances obtained from photographic high-dispersion spectra (Cohen 1983). However, from more than 160 giants homogeneously analyzed in 24 calibrating clusters, CG96 have demonstrated that the ZW metallicities differ significantly from these new results. In particular, they are about 0.10 dex higher for $[\text{Fe}/\text{H}] > -1$, 0.23 dex lower for $-1 < [\text{Fe}/\text{H}] < -1.9$, and 0.11 dex too high for $[\text{Fe}/\text{H}] < -1.9$. This non-linearity of the ZW scale is significant at 3σ level and cannot be ignored when discussing astrophysical problems involving tiny metallicity differences among the clusters.

On the basis of the CG96 new scale, Carretta and Gratton (1996b) have also derived a new calibration of $(B - V)_{o,g}$ in terms of $[\text{Fe}/\text{H}]$. Using the values of $(B - V)_{o,g}$ from the compilation of Michel and Smith (1984) for 22 calibrating cluster on the new scale, they obtained a 2^{nd} -order polynomial fit that closely resembles the theoretical calibration of Demarque *et al.* (1982) from evolutionary red-giant models. Based on this new calibration, the metallicity of M 3 turns out to be $[\text{Fe}/\text{H}] = -1.38$, with a 1σ error bar of 0.18 dex, in good agreement with the spectroscopic determination reported by CG96.

In conclusion, from the detailed re-analysis discussed above, we are inclined to believe that the metallicity of M 3 is slightly larger than estimated so far and probably the best value to adopt at present is $[\text{Fe}/\text{H}] = -1.45 \pm 0.10$, where both the absolute figure and the size of the error are just the result of our global overview.

3.3. The bump on the Red Giant Branch

Theoretical evolutionary models predict the existence of a special feature along the RGB called the “RGB-bump” (see e.g. Thomas 1967, Iben 1968, RFP88). As discussed in detail among others by Rood and Crocker (1985), the practical detection of such a feature requires the availability of very populous RGB samples. Fusi Pecci *et al.* (1990) detected the RGB-bump in 11 globular clusters, including M 3 (based on our early PH94 data; see also Ferraro 1992). The use of our new data-base allows us to confirm the detection of the RGB-bump (see Figure 4, Figure 17) located at $V_{\text{bump}} = 15.45 \pm 0.05$, i.e. exactly the same value as the previous measurement listed in Table 4 of Fusi Pecci *et*

al. (1990), and we thus refer to that paper for the discussion of this specific issue.

Fig. 17. Integrated (panel a) and differential (panel b) luminosity functions of the RGB (Bright Complete Sample). The vertical line in panel (b) shows the location of the *RGB-bump*.

3.4. The HB population and morphology in M 3

Based on our bright sample, containing *all* the stars brighter than $B = 18.6$ and located within a square of about $7' \times 7'$ (but with $r > 20''$), the HB of M 3 spans a very wide colour range (~ 1 mag), from the red end at $B - V \sim 0.7$ to the bluest stars at $B - V \sim -0.3$. Therefore the distribution in effective temperature is very wide, and, in turn, there is a wide spread in the HB mass distribution (Rood and Crocker 1985).

Recently, Fusi Pecci *et al.* (1992, 1993) have discussed in detail the properties of the observed HB morphologies (and in particular the so-called “Second Parameter” problem) in relation to stellar mass loss, the effect of the environment on the evolution of the individual stars, and the presence of binary systems (primordial, collisional, merging, etc.). In particular, the HB of M 3 has been *dissected* into sub-groups having presumably different evolutionary histories. The basic idea is that both the blue and the red extremes of the observed HB might include peculiar objects which are intrinsically different from *genuine* HB stars and are rather the result of the stellar and dynamical evolution of binary systems (at least in part related to the blue stragglers), or are HB objects which keep track of interactions causing an “extra-mass loss” from the envelope during the previous evolutionary stages.

For the sake of brevity we refer to the quoted papers for a complete discussion and simply re-analyse the content of the boxes which have been defined in PH94 to describe the HB morphology.

Fig. 18. Enlargement of the colour-magnitude diagram of M 3 in the HB region, with boxes defining the areas we identified along the HB. All stars belonging to our BCS sample are plotted in this Figure apart from the 186 known variables (see text).

As show in Figure 18 we have “dissected” the HB into seven boxes and report below a few notes on each sub-group.

1. *Group HEB*: 10 stars (2 in PH94), the faintest one reaching $V \sim 18.3$ and with $B - V < -0.1$, but a few other bluer and/or fainter objects might deserve a further check. Their location in the CMD could well be

due to large photometric errors or they could be non-members. Most of them are confined within the inner 2 arcmin from the cluster center. If their photometry and membership are confirmed, they could represent good candidates to search for the possible descendants of late collisional mergers (Bailyn and Iben 1989, Fusi Pecci *et al.* 1992) or they could be post-HB stars (such as AGB-manquè, see e.g. Greggio and Renzini 1990, Cacciari *et al.* 1995, D’Cruz *et al.* 1996).

2. *Group EB*: 10 stars (4 in PH94). Together with the 10 HEB stars, this group constitutes a subset of 20 stars clearly segregated from the bulk of the HB stellar population. Their total number and location seems sufficient to exclude the possibility that all of them are interlopers. Hence, we are inclined to conclude that there is now clear-cut observational evidence for the existence of a very extended (though sparsely populated) blue HB tail in M 3, possibly separated by a gap from the bulk of the *normal* HB objects. The *HST* UV data currently being analyzed, coupled with spectroscopy, could be very helpful in understanding their true origin.
3. *Group B*: 206 objects, (70 in PH94). The population of this box includes presumably *normal* HB stars located above a small (apparent?) gap at $V \sim 16.9$ and bluer than the blue edge of the instability strip. The scatter of the points around the mean ridge line is compatible with the size of the observational errors (note that the B exposures are short), but it could also partially reflect the effects due to evolution off the ZAHB for some stars.
4. *Group V*: 186 stars (85 in PH94). This group contains only RR Lyrae variables. In Figure 18 variables are not reported as appropriate mean values are still lacking. At present, mean V and $B - V$ values are listed for the 85 HB variables of the photographic sample in Table 10 of PH94. For the other 100 HB variables mean magnitudes and colours are not available from the present photometric data. Consequently, their presence in the plotted CMD would introduce a “confusing” scatter of the points both in magnitude and in colour mostly due to a random-phase effect of the available measurements, which are insufficient to cover completely the light curve.
A few of these stars could however also be evolved HB stars brighter than the ZAHB. Finally, there are 17 constant stars which are located within the box because of photometric errors or due to the existence of some overlapping in colour of the variable and non-variable strips. This specific item will be dealt with in more details in a forthcoming paper. However, we have included them in the total number of HB stars.
5. *Group R*: 106 stars (51 in PH94). They lie to the red of the instability strip and reach up to about half a magnitude brighter and redder than the ZAHB level within the instability strip.

6. *Group ER*: 15 stars (7 in PH94). This group overlaps in colour with the previous one, but it is composed of stars brighter than $V \sim 15.3$ and still well separated from the AGB base. As mentioned in PH94, at least some of them could be the “progeny” of BSS (see Fusi Pecci *et al.* 1992) and they are thus worth of further study.
7. *Group SHB*: 7 stars. They are located well above the HB and could represent *highly evolved* HB objects which are travelling from their original ZAHB location towards the AGB. Alternatively, they could be blends of HB+RGB stars.

3.5. Star counts and population ratios: mixing and He abundance

A complete sample of stars with accurate photometry offers a major tool for an observational verification of the predictions of the stellar evolution theory. In particular, star counts in a given evolutionary phase yield a direct test of the duration of that specific phase (Renzini and Buzzoni 1986). In turn, this allows one to get a deeper insight on unsolved problems like for instance the extent of the mixing phenomena, or to measure important basic quantities like the primordial helium abundance Y (see RFP88).

The approach to the problem is well established (see e.g. RFP88, PH94): from the CMD one can measure a set of parameters to be used along with the appropriate calibrations based on theoretical models. The most frequently used are:

- $R = N_{HB}/N_{RGB}$, the ratio of the numbers of stars on the HB and on the RGB brighter than ZAHB luminosity at $\text{Log}T_e \sim 3.85$;
- $R' = N_{HB}/(N_{RGB} + N_{AGB})$, which includes also the number of stars in the AGB phase;
- $R1 = N_{AGB}/N_{RGB}$;
- $R2 = N_{AGB}/N_{HB}$.

To preserve full homogeneity with the study of Buzzoni *et al.* (1983, BFBC) which is still the standard reference for this subject, we have adopted their prescriptions. In particular, we fixed the separation between HB and AGB at $V \simeq 14.9$, about 0.8 mag above the mean magnitude of the HB, and counted RGB stars brighter than $V = 15.81$, adopting a differential bolometric correction $\Delta B.C. = 0.11$ mag (O. Straniero, private communication) between HB and RGB stars. The results for the star counts along the various branches and the derived parameters are listed in Table 4.

The parameters $R1$ and $R2$ essentially indicate the relative ratios of the lifetimes of the AGB, RGB, and HB. Since these lifetimes are basically driven by nuclear burning and mixing phenomena (which may alter the “local” fuel quantity), different ratios are predicted from the models with varying mechanisms and extension of mixing for

Table 4. Star counts on HB, AGB, and RGB of M 3

N_{RGB}	= 414
N_{HB}	= 550
N_{AGB}	= 69
R	= 1.33 ± 0.12
R'	= 1.14 ± 0.10
$R1$	= 0.17 ± 0.03
$R2$	= 0.12 ± 0.02

Note: all counts and ratios refer to our Bright Complete Sample (BCS).

fixed properties of the nuclear burning. Within the framework discussed by RFP88, the values here obtained for $R1$ and $R2$ are fully compatible with the predictions of “standard and canonical” models.

The values for R and R' can be used along with eqs. 11 and 13 of BFBC to obtain an estimate of the primordial He abundance based on their calibrations of these parameters in terms of Y . From the values listed in Table 4 (the errors are just from count statistics), we obtain $Y_R = 0.22 \pm 0.02$ and $Y'_R = 0.23 \pm 0.02$, in excellent agreement with the mean value found by BFBC as well as with other estimates (see e.g. Boesgaard and Steigman 1985, Olive and Steigman 1995 and ref. therein). In the computation we have considered for the HB all the stars included in the samples ER+R+V+R+EB+HEB. This may not be fully correct if at least some of them are *non-genuine* HB stars (in the sense that they are not evolving “directly” from the RGB). However, since their number (including the few SHB stars) is so small, the result is practically unaffected taking into account the size of the errors. For instance, by deleting from the HB all the stars in the samples ER+EB+HEB, the computed ratios would become $R = 1.24$, $R' = 1.07$, $R1 = 0.17$, $R2 = 0.13$, which would leave the conclusions on Y unchanged.

3.6. The Blue Stragglers population of M 3: toward the definition of a complete and reliable sample

A comprehensive discussion on the BSS population of M 3 has already been presented in F93. Therefore, here we shall only extend to the BSS region the same kind of comparisons with the data-sets of other previous studies in order to verify the quality of the different samples in terms of completeness and selection bias. We anticipate that the problem of identifying a truly pure sample of BSS candidates is far from being solved, in particular in the inner regions of the clusters where crowding undermines photometry and for the faint BSS, whose separation from *normal* TO stars is always difficult and somewhat subjective.

We report below identifications and comparisons made with respect to BHS for the region in common with our newly re-calibrated CFHT CCD data. The comparison

will be based on V and I colours only, because of the poor response of the chip used for the observations in the B filter.

Figure 19 shows the result of the comparison with the sample obtained by BHS for $r > 20''$. *Panel (a)* shows the data from BHS (kindly made available to us by Dr. M. Bolte) with their instrumental magnitudes shifted to our system. The box reproduces the polygonal region used by BHS (their Figure 3) for selecting their BSS candidates. Open squares are the stars in the BHS sample that are the counterparts of our BSS candidates on the BHS field. *Panel (b)* displays our CCD-sample, restricted to the BHS field. The box is the same as we used to delimitate the region occupied by our (F93) BSS candidates and is identical to that in Figure 3 of F93. Open squares are the stars of our sample which are counterparts of the BSS candidates selected by BHS and falling outside our adopted limits. In both panels, black squares represent stars that are considered BSS by both surveys.

As can be seen, there are only 15 BSS candidates in common (the black squares), while there are 50 stars labeled as BSS candidates in only one of the two surveys. Could all of them be mis-selected; could they actually be *normal* stars? The answer is difficult to find, but some additional considerations may be useful.

Our 25 BSS candidates not identified as such by BHS mostly fall between their BSS box and their SGB. Judging on the basis of the scatter in the TO region, our photometry seems to display smaller internal errors. This may indicate that we can better separate the two populations because of the different quality of the photometry. Another obvious explanation is, of course, that we reached too close to the MS in defining our BSS box. On the other hand, the 10 stars identified as BSS candidates only by BHS fall in *panel (b)* of Figure 19 at somewhat brighter magnitudes than the TO region. Since the quality of the CCD frames available to BHS seems to be better as far as seeing conditions are concerned, this might imply that we were unable to separate the optical blends formed by a BSS-candidate and a SGB star. *HST*-data should be suitable to settle the issue.

Fig. 19. Comparison of the BSS found in our sample and in BHS study. In panel (a) are plotted the data from BHS, with instrumental magnitudes shifted to our system. The box reproduces the polygonal region used by BHS (their Figure 3) for selecting their BSS candidates. Open squares are the stars in BHS sample that are the counterparts of our BSS candidates on the BHS field. Panel (b) shows our CCD sample, restricted to the BHS field; the box is the same we used to encircle the region occupied by our BSS candidates (Figure 3 of F93). Open squares are the stars of our sample which are counterparts of BHS BSS candidates. In both panels, black squares represent stars that are considered BSS by both surveys.

4. Summary and Conclusions

We have presented the BVI CCD data for about 10,000 stars in the region $0.3' < r < \sim 4'$ of M3. These data, along with our previous photographic photometry of additional $\leq 10,000$ stars in the external regions as far as $7'$, provide a homogeneous and populous data base for detailed population studies. Completeness has been achieved for all objects with $V \leq 18.6$.

Our main results are:

- A new absolute photometric calibration has been obtained. The comparison with the absolute calibration adopted so far for the same field (Sandage and Katem 1982) shows that there is a significant colour term, in the sense that our calibration is ~ 0.07 mag redder than Sandage and Katem (1982) in the blue range e.g. at $B-V = -0.2$, slightly redder (~ 0.03 mag) at the instability strip, and ~ 0.08 mag bluer in the reddest part of the CMD, e.g. at $B-V = 1.6$. This has important implications in the photometric determination of the metallicity, and in other items such as the period-shift effect which will be discussed in a forthcoming paper.
- After completion of our reductions, we became aware of the availability of a new independent photometry of a very wide sample of M3 stars (about 23,700) carried out by K.A. Montgomery (1995 – M95), fully overlapping our considered regions. The use of this new catalog has also allowed us to get a link to the photometry presented by Stetson and Harris (1988) for an external area, outside our surveyed region. In synthesis, there are now three independent calibrations referred to observations of Landolt's (1992) standards. They are in marginal agreement, but it is difficult at the present stage to choose which is the best. Since the calibration here adopted seems to be compatible with that obtained by Stetson and Harris (1988) (they actually show a systematic difference of 0.04 both in B and V, yielding however no colour difference), we decided to keep using our new calibration.
- Based on these new data and calibration, the metallicity derived from the photometric indicators $(B - V)_{0,g}$ and $\Delta V_{1,4}$ is $[\text{Fe}/\text{H}] \sim -1.45$. This value is significantly higher than the value -1.66 commonly used for M3, and is in very good agreement with the most recent metallicity determinations from high resolution spectroscopy of individual stars.
- Evidence has been found of the presence of a faint and blue extension of the HB, although scarcely populated. These stars, however, could be non-genuine HB members but rather the results of merging or collisions. More photometric and spectroscopic work is needed in order to assess the true nature of these objects.
- From the population ratios of HB, RGB and AGB stars we find a value for the helium content $Y = 0.23 \pm 0.02$. This confirms the previous determinations of helium content in globular clusters by this method.

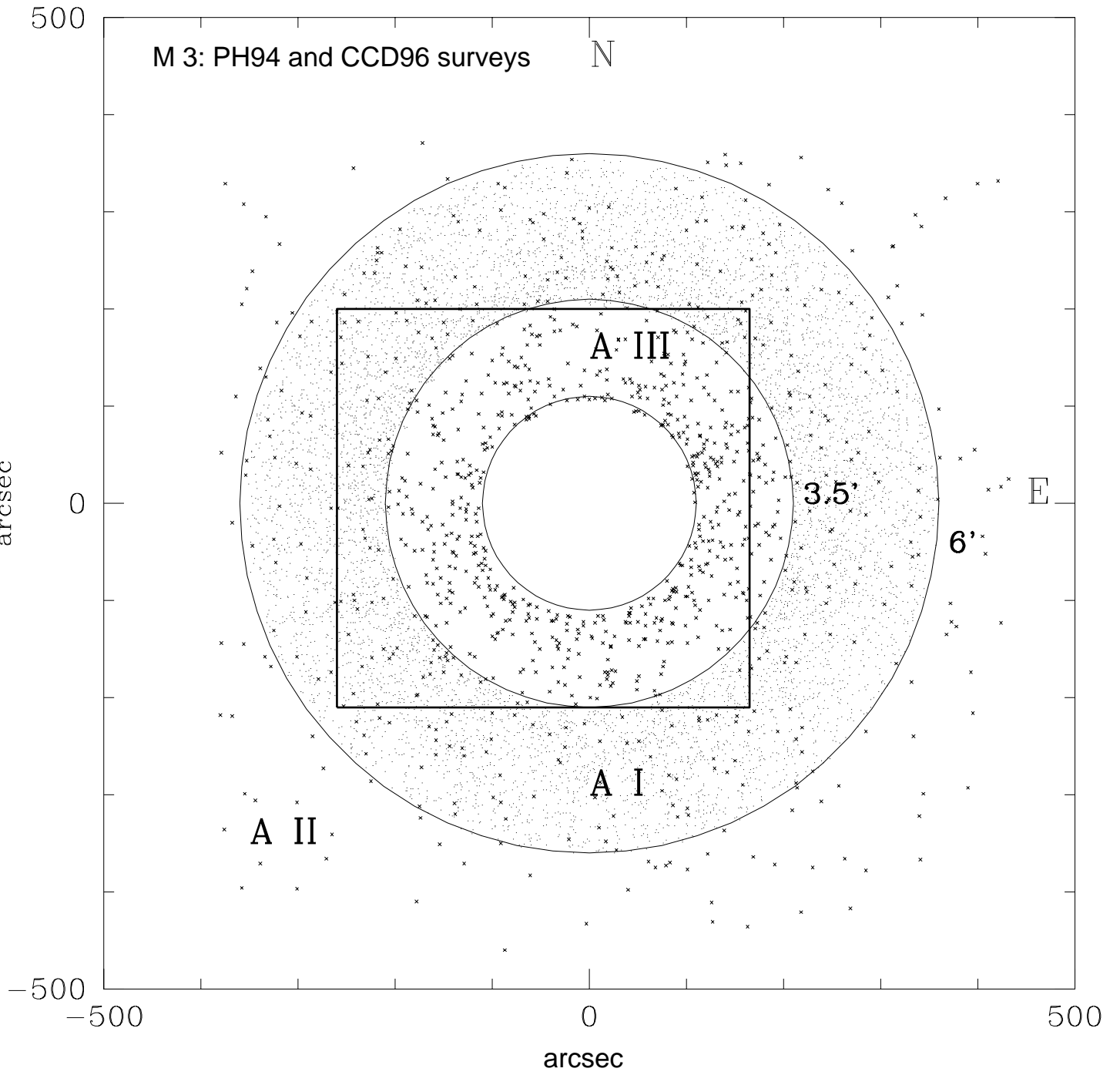
- A significant population of blue straggler stars has been detected and identified. However the exact number of BSS must await HST data for a better space resolution in the most internal regions, for resolving optical blends that may turn pairs of TO stars into BSS, and in general for a better photometric accuracy. Spectroscopic follow-up studies will be extremely important for a better understanding of the formation mechanisms of these stars.

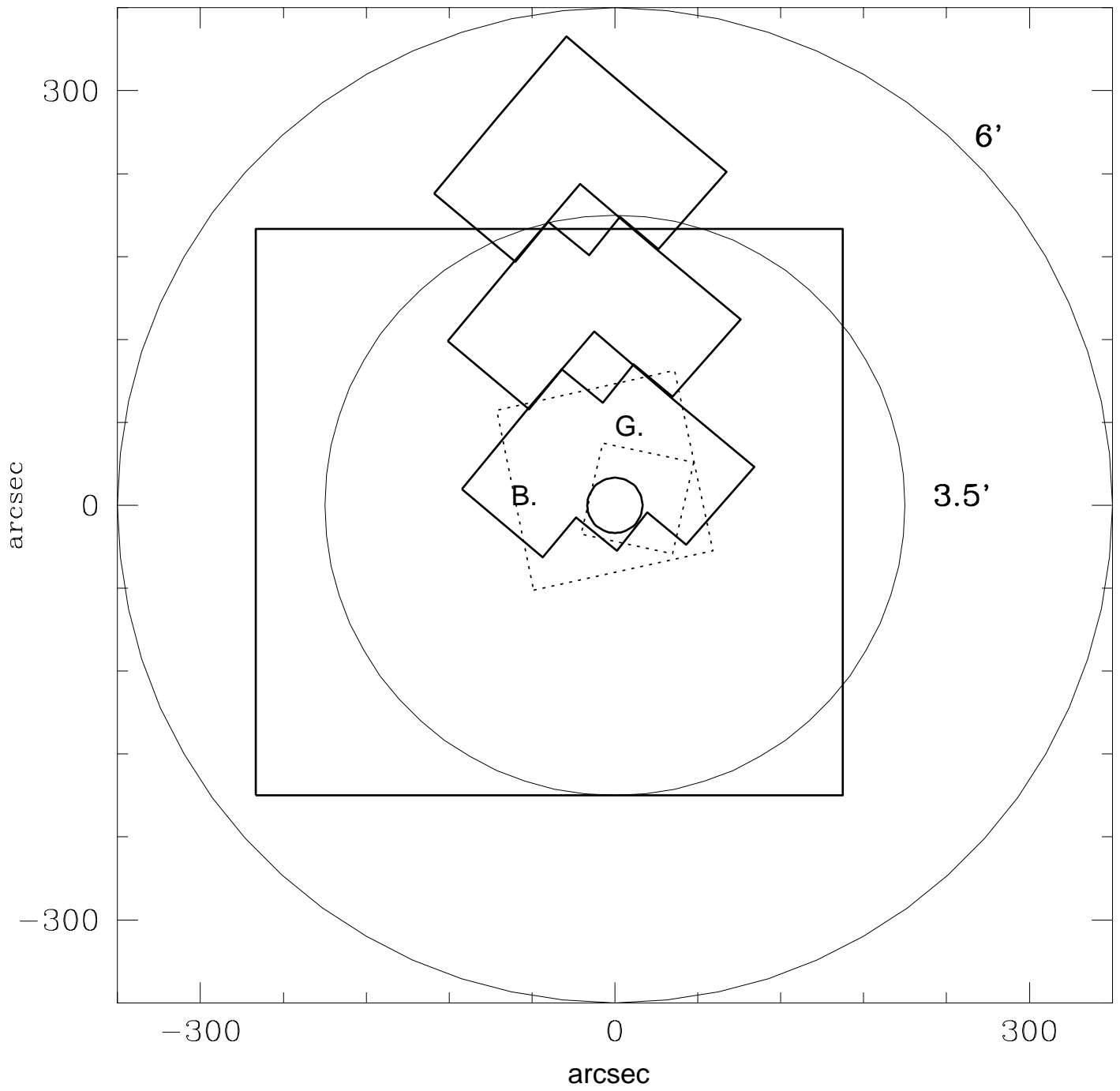
Acknowledgements. We wish to thank H. Richer and G. Fahlman for their collaboration in taking the observations at the CFHT. We are grateful to the CFHT and the Calar Alto Observatories for the kind hospitality and support provided during the observations. We are specially indebted to K. Janes for providing us with his independent sample of M 3 stars in advance of publication, which has allowed us to perform important tests and corrections, and M. Bolte for providing us with his data on Blue Stragglers stars. We are pleased to acknowledge R.T. Rood for his critical reading of the manuscript and several useful comments and suggestions. This work has been supported by the Italian Ministry for Research (MURST).

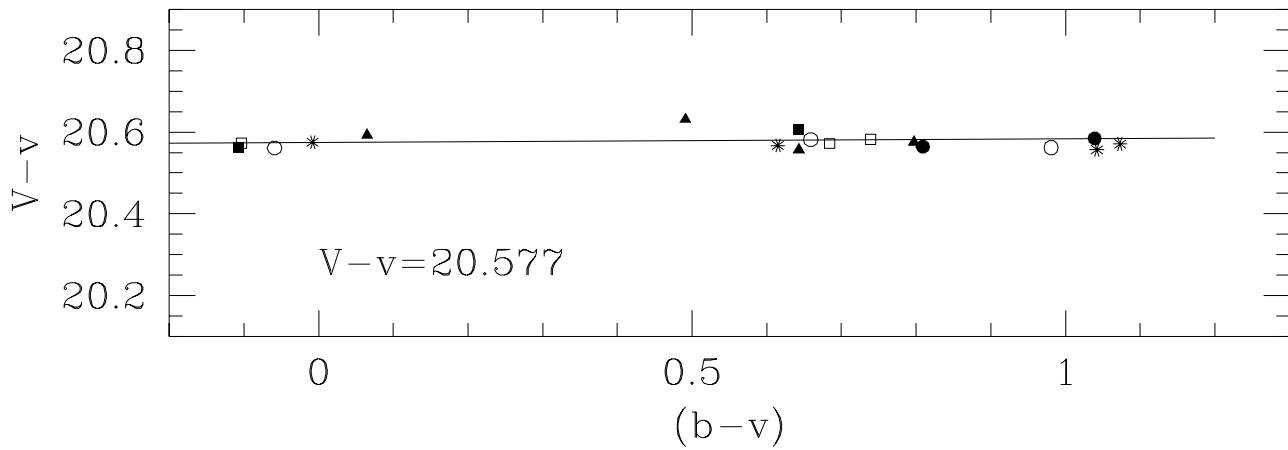
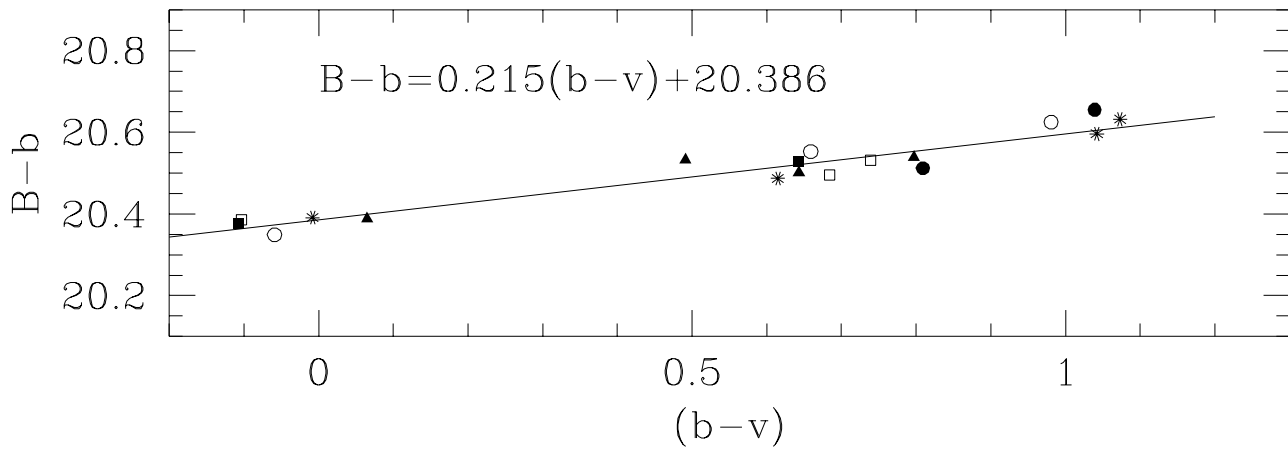
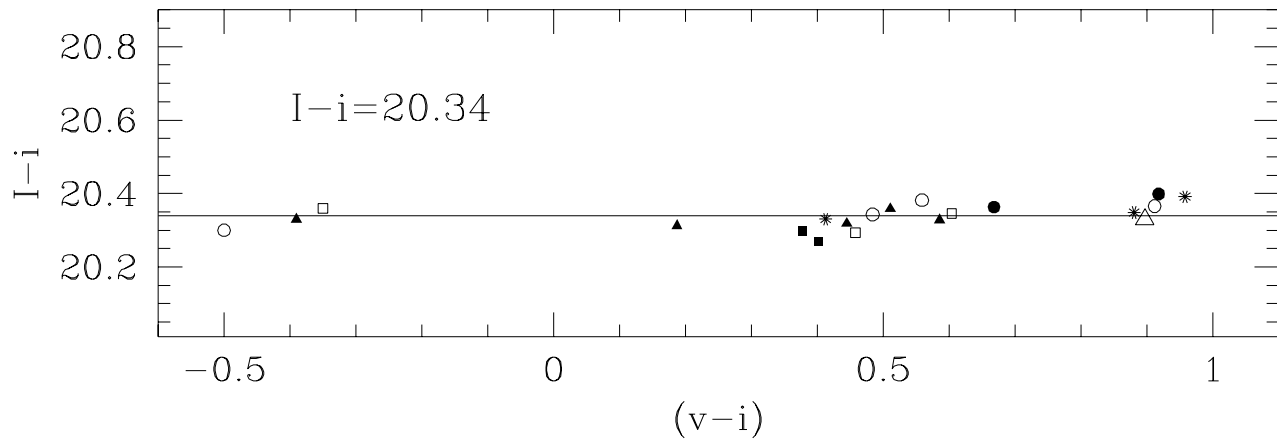
References

- Aurière, M., Cordoni, J.P. 1983, A&AS, 52, 383
 Baily, C.D., Iben, I.Jr. 1989, Ap.J., 347, L21
 Bell, R.A., Eriksson, K., Gustafsson, B., Nordlund, A. 1976, A&AS, 23, 37
 Boesgaard, A., Steigman, G. 1985, A.R.A.A., 23, 319
 Bolte, M., Hesser, J.E., Stetson, P.B. 1993, ApJL, 408, L89 (BHS)
 Buonanno, R., Corsi, C.E., De Biase, G.A., Ferraro, I. 1979, in *Image Processing in Astronomy*, eds. G. Sedmak, M. Cappacioli & R.J. Allen, Trieste, Italy, p.354
 Buonanno, R., Buscema, G., Corsi, C.E., Ferraro, I., Iannicola, G. 1983, A&A, 126, 278
 Buonanno, R., Buzzoni, A., Corsi, C.E., Fusi Pecci, F. Sandage, A.R. 1986, Mem.SAI, 57, 391
 Buonanno, R., Corsi, C.E., Buzzoni, A., Cacciari, C., Ferraro, F.R., Fusi Pecci, F. 1994, A&A, 290, 69 (PH94)
 Burgarella, D., Paresce, F., Quilichini, V. 1995, A&A, 301, 675
 Buzzoni, A., Fusi Pecci, F., Buonanno, R., Corsi, C.E., 1983, A&A, 301, 675
 Cacciari, C. et al. 1996, in preparation
 Cacciari, C., Fusi Pecci, F., Bragaglia, A., Buzzoni, A. 1995, A&A, 301, 684
 Cacciari, C., Carretta, E., Ferraro, F.R., Fusi Pecci, F., Tesicini, G., Nemeč, J., Walker, A.R. 1993, in *New Perspectives on Stellar Pulsation and Pulsating Variable Stars*, J.Nemeč, J. Matthews eds. Cambridge Univ. Press, IAU Coll. 139, 325
 Carretta, E., Gratton, R.G. 1996a, A&AS, in press (CG96)
 Carretta, E., Gratton, R.G. 1996b, A&A, in preparation
 Cohen, J.G. 1983, ApJ, 270, 654
 Costar, D., Smith, H.A. 1988, AJ, 96, 1925
 D'Cruz, N., Dorman, B., Rood, R.T., O'Connell, R.W. 1996, preprint
 Demarque, P., King, C.R., Diaz, A. 1982, ApJ, 259, 154
 Ferraro, F.R. 1992, Mem.SAI., 63, 491

- Ferraro, F.R., Clementini, G., Fusi Pecci, F., Buonanno, R., Alcaino, G. 1990, *A&AS*, 84, 59
- Ferraro, F.R., Clementini, G., Fusi Pecci, F., Sortino, R., Buonanno, R. 1992b, *MRAS*, 256, 391
- Ferraro, F.R., Fusi Pecci, F., Buonanno, R. 1992a, *MNRAS*, 256, 376
- Ferraro, F.R., Fusi Pecci, F., Cacciari, C., Corsi, C., Buonanno, R., Fahlman, G.G., Richer, H.B. 1993, *AJ*, 106, 2324 (F93)
- Fusi Pecci, F., et al. 1996, in preparation
- Fusi Pecci, F., Ferraro, F.R., Crocker, D.A., Rood, R.T., Buonanno, R., 1990, *A&A*, 238, 95
- Fusi Pecci, F., Ferraro, F.R., Bellazzini, M., Djorgovski, D.S., Piotto, G., Buonanno, R., 1993, *AJ*, 105, 1145
- Fusi Pecci, F., Ferraro, F.R., Corsi, C.E., Cacciari, C., Buonanno, R. 1992, *AJ*, 104, 1831
- Gratton, R.G. 1987, *A&A*, 179, 181
- Gratton, R.G., Ortolani, S. 1989, *A&A*, 211, 41
- Greggio, L., Renzini, A. 1990, *ApJ*, 364, 35
- Guhathakurta, P., Yanny, B., Bahcall, J.N., Schneider, D.P. 1994, *AJ*, 108, 1786 (GYBS)
- Holweger, H., Müller, E.A. 1974, *Solar Phys.*, 39, 19 (HM)
- Iben, I.Jr. 1968, *Nature*, 220, 143
- King, I.R. 1966, *AJ*, 71, 64
- Kraft, R.P., Sneden, C., Langer, G.E., Shetrone, M.D., Bolte, M. 1995, *AJ*, 109, 2586
- Kurucz, R.L., 1992, private communication
- Landolt, A.U. 1983, *AJ*, 88, 439
- Landolt, A.U. 1992, *AJ*, 104, 340
- Lee, Y.W., Demarque, P., Zinn, R.J. 1990, *ApJ*, 350, 155
- Leep, E.M., Oke, J.B., Wallerstein, G. 1987, *AJ*, 93, 338
- Michel, A., Smith, H.A. 1984, *PASP*, 96, 588
- Montgomery, K.A. 1995, Ph.D Thesis, Boston University
- Olive K.A., Steigman, G. 1995, *ApJS*, 97, 49
- Oosterhoff, P.T. 1939, *Observatory*, 39, 104
- Paez, E., Straniero, O., Martinez Roger, C. 1990, *A&AS*, 84, 481
- Renzini, A., Buzzoni, A. 1986, in *Spectral Evolution of Galaxies*, C. Chiosi and A. Renzini eds., (Reidel, Dordrecht), 135
- Renzini, A., Fusi Pecci, F. 1988, *ARA&A*, 26, 199 (RFP88)
- Rood, R.T., Crocker, D.A. 1985, in *Production and Distribution of CNO Elements*, I.J. Danziger, F. Matteucci, K. Kjær eds., (Garching:ESO), p. 961
- Sandage, A.R. 1953, *AJ*, 58, 61
- Sandage, A.R. 1970, *ApJ*, 162, 841
- Sandage, A.R. 1993, *AJ*, 106, 703
- Sandage, A.R., Katem, B. 1982, *AJ*, 87, 537
- Sandage, A.R., Smith, L.L. 1966, *ApJ*, 144, 886
- Sandage, A.R., Wallerstein, G. 1960, *ApJ*, 131, 598
- Sarajedini, A. 1994, *AJ*, 107, 618
- Scholtz, R.-D., Kharchenko, N.V. 1994, *Astron. Nachr.*, 1, 73
- Sneden, C., Kraft, R.P., Prosser, C.F., Langer, G.E. 1992, *AJ*, 104, 2121 (SKPL)
- Sweigart, A.V., Gross, P.G. 1976, *ApJS*, 32, 367
- Sweigart, A.V., Renzini, A., Tornambè, A. 1987, *ApJ*, 312, 762
- Thomas, H.C. 1967, *Z. Astrophys.*, 67, 420
- Zinn, R.J., West, M.J. 1984, *ApJS*, 55, 45





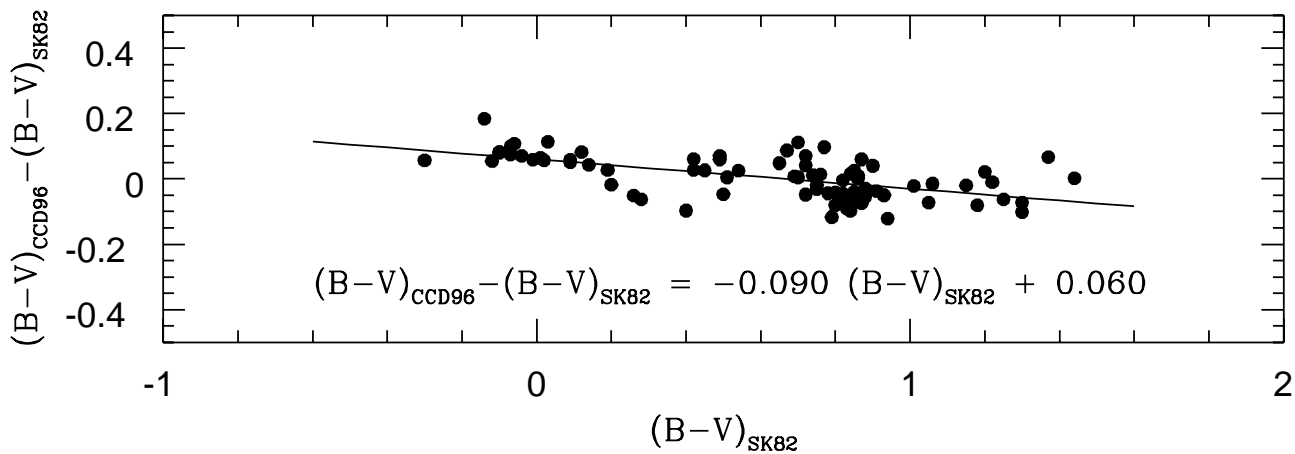
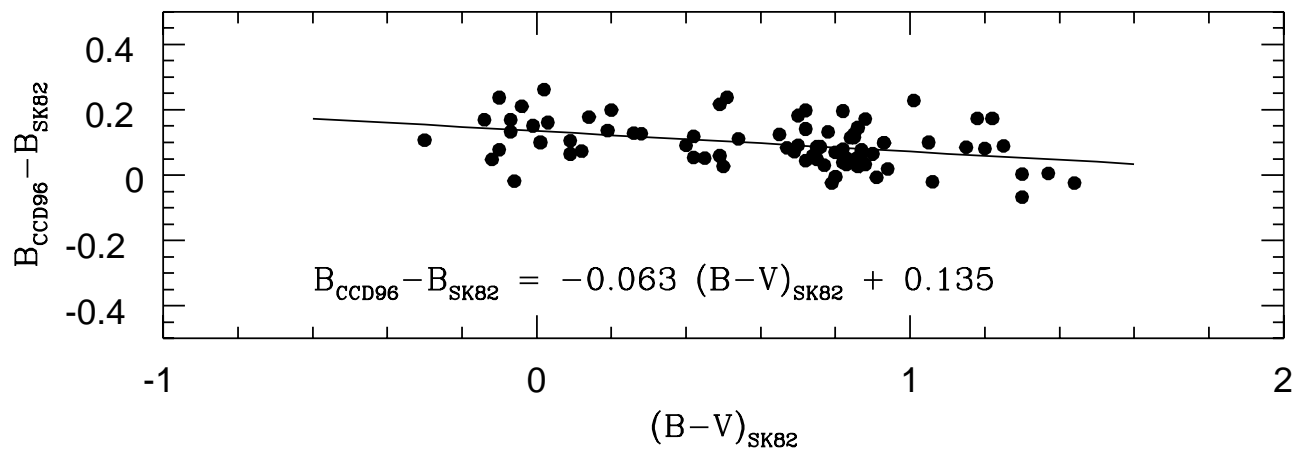
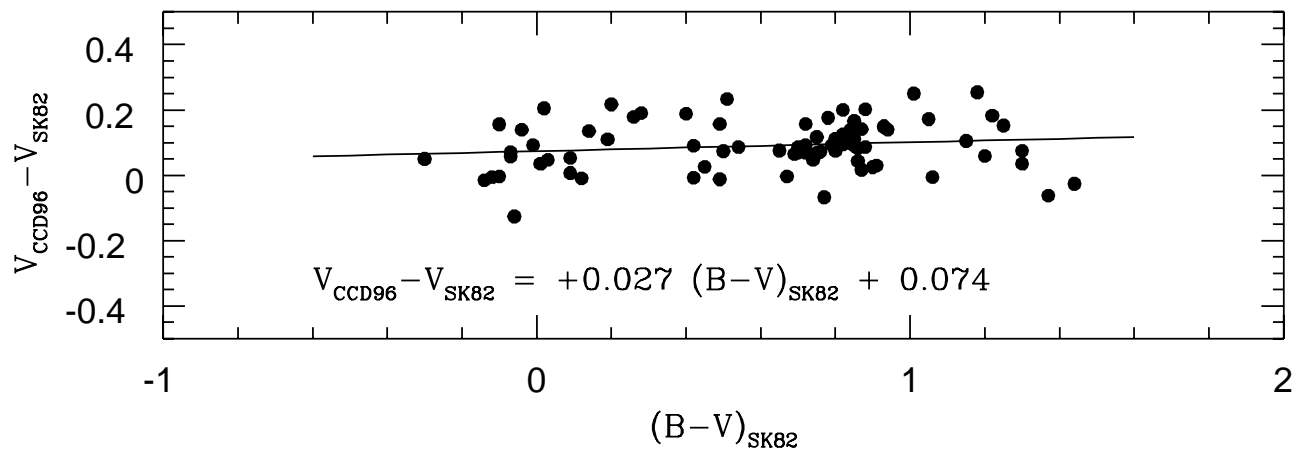


This figure "5478f4.gif" is available in "gif" format from:

<http://arxiv.org/ps/astro-ph/9611016v1>

This figure "5478f5.gif" is available in "gif" format from:

<http://arxiv.org/ps/astro-ph/9611016v1>

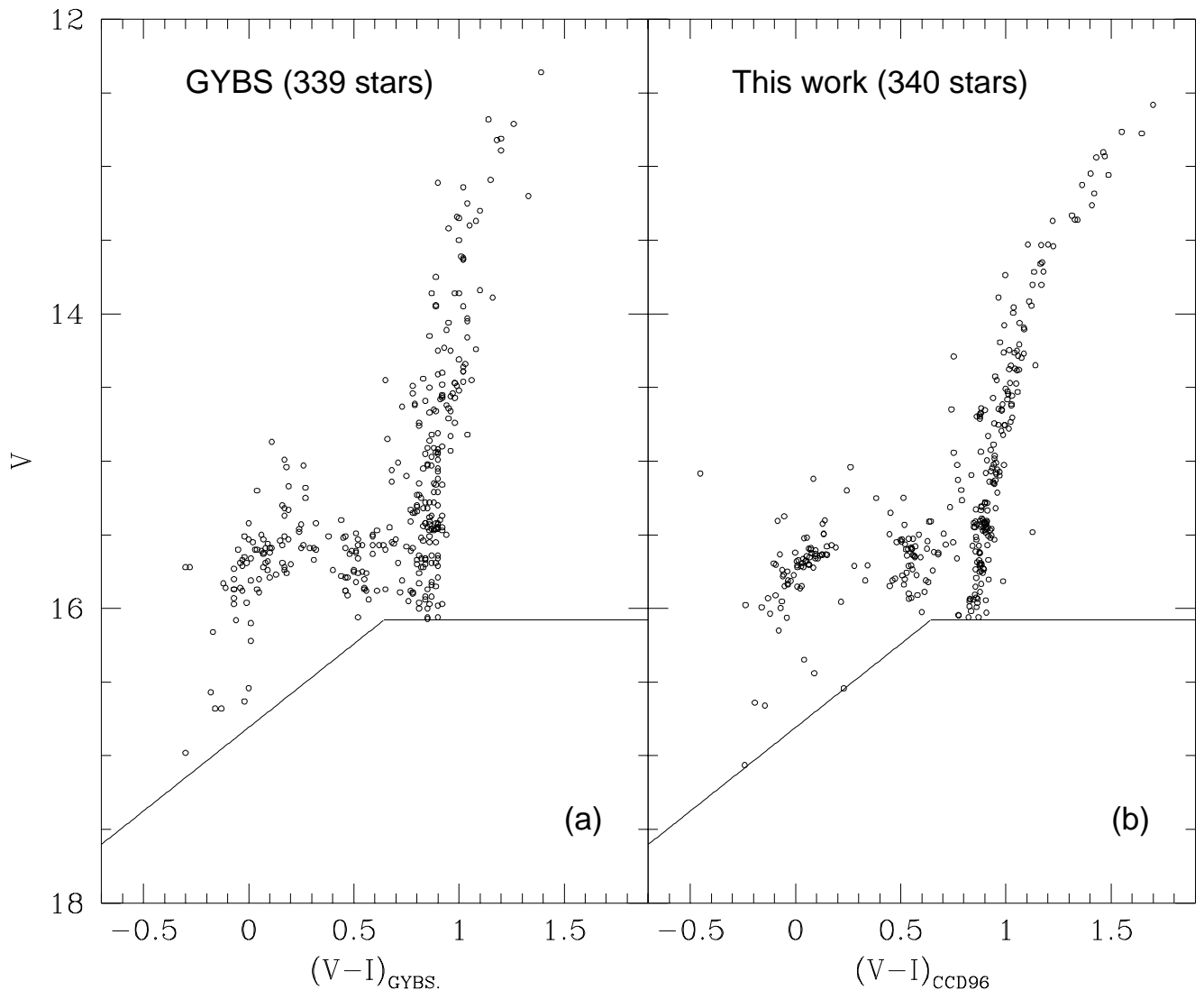


This figure "5478f7.gif" is available in "gif" format from:

<http://arxiv.org/ps/astro-ph/9611016v1>

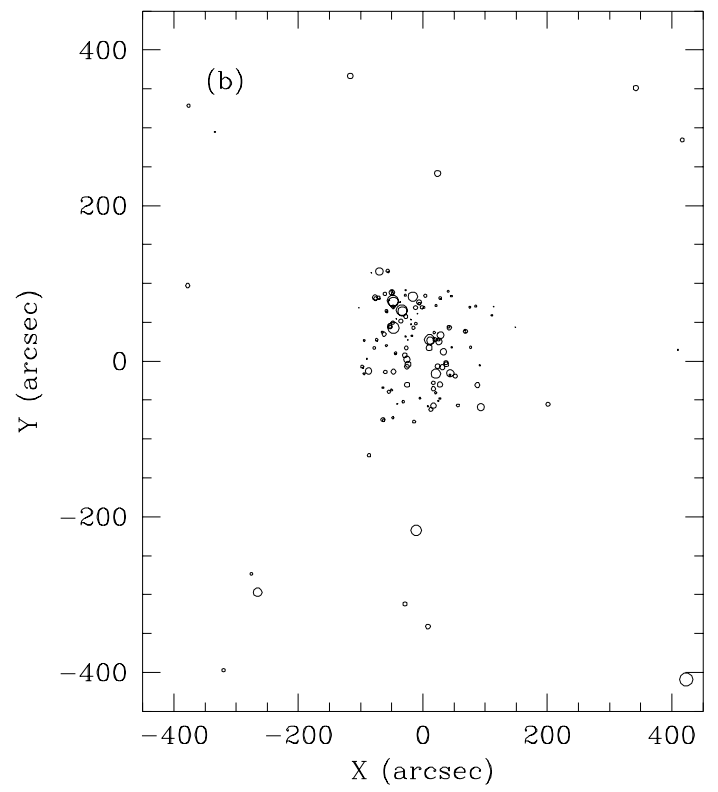
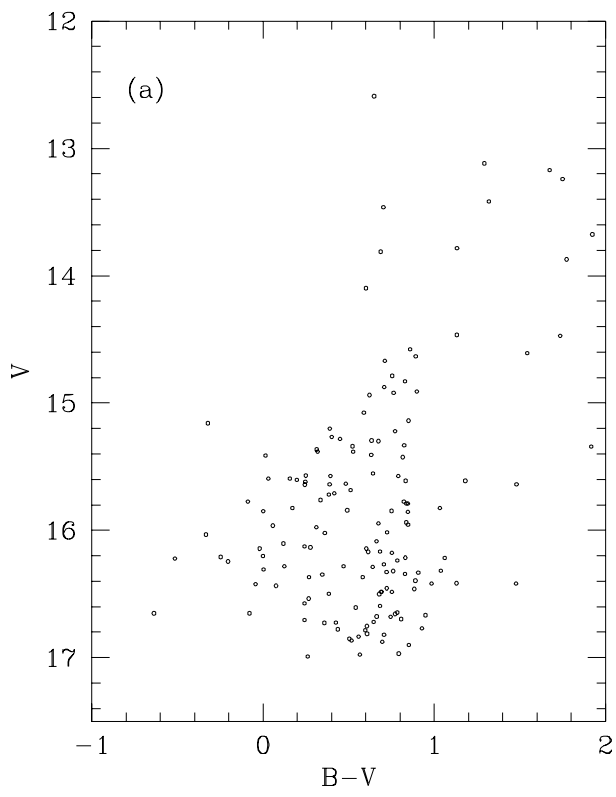
This figure "5478f8.gif" is available in "gif" format from:

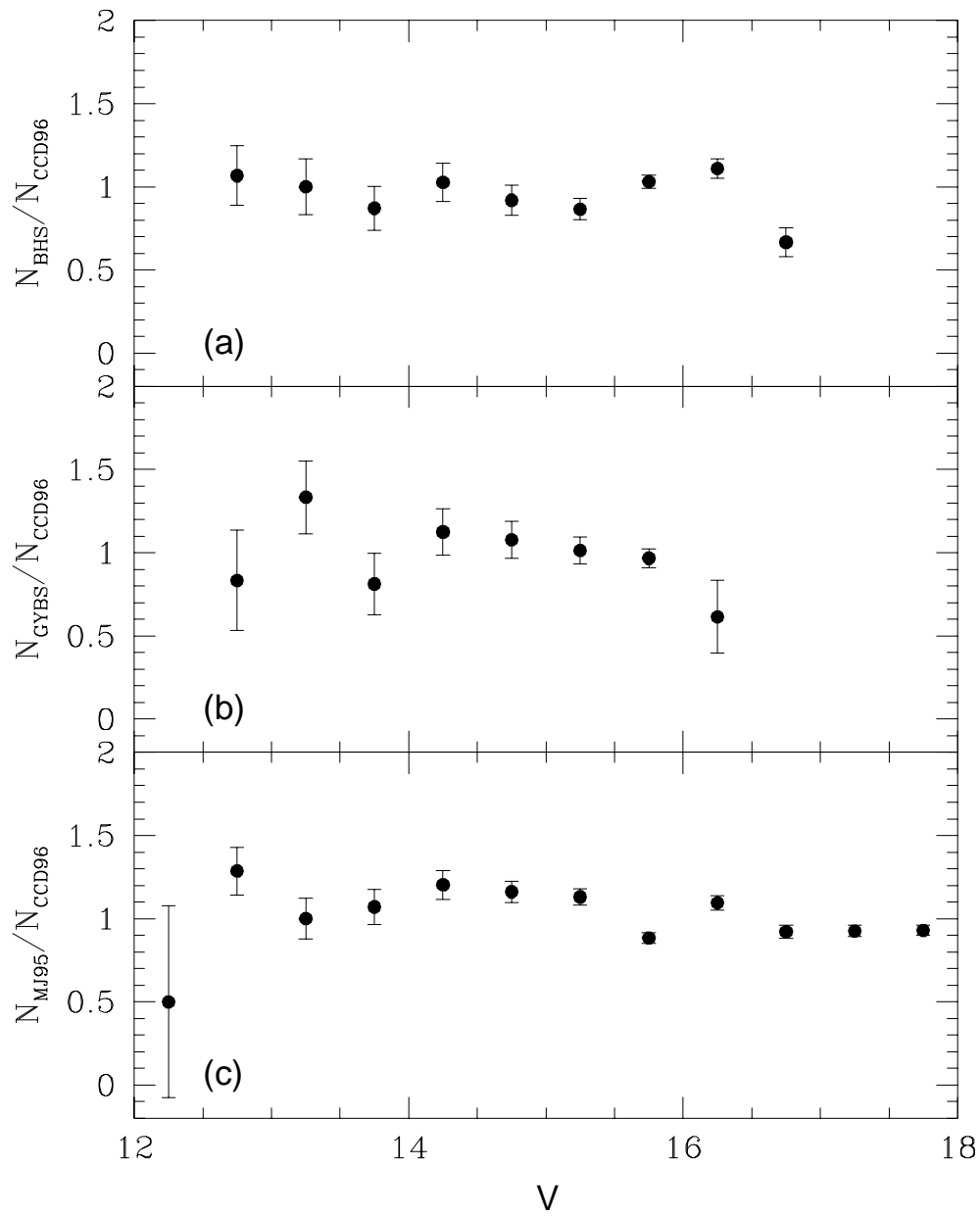
<http://arxiv.org/ps/astro-ph/9611016v1>



This figure "5478f10.gif" is available in "gif" format from:

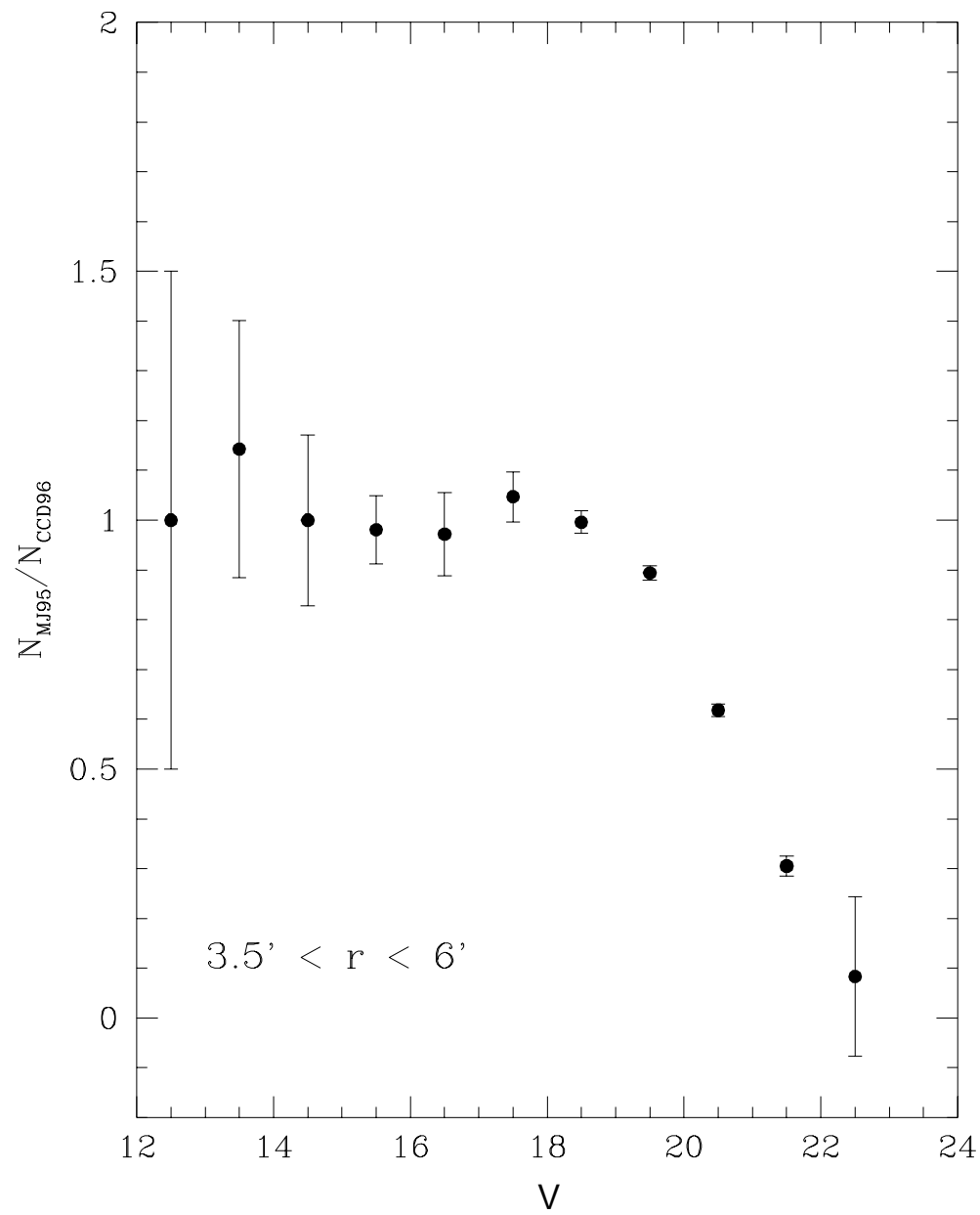
<http://arxiv.org/ps/astro-ph/9611016v1>





This figure "5478f13.gif" is available in "gif" format from:

<http://arxiv.org/ps/astro-ph/9611016v1>

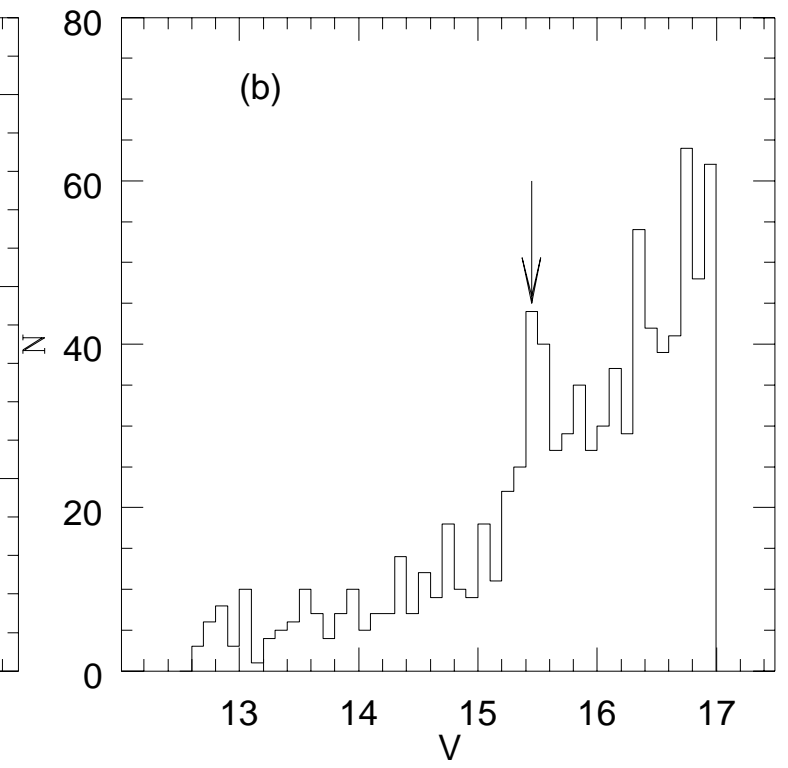
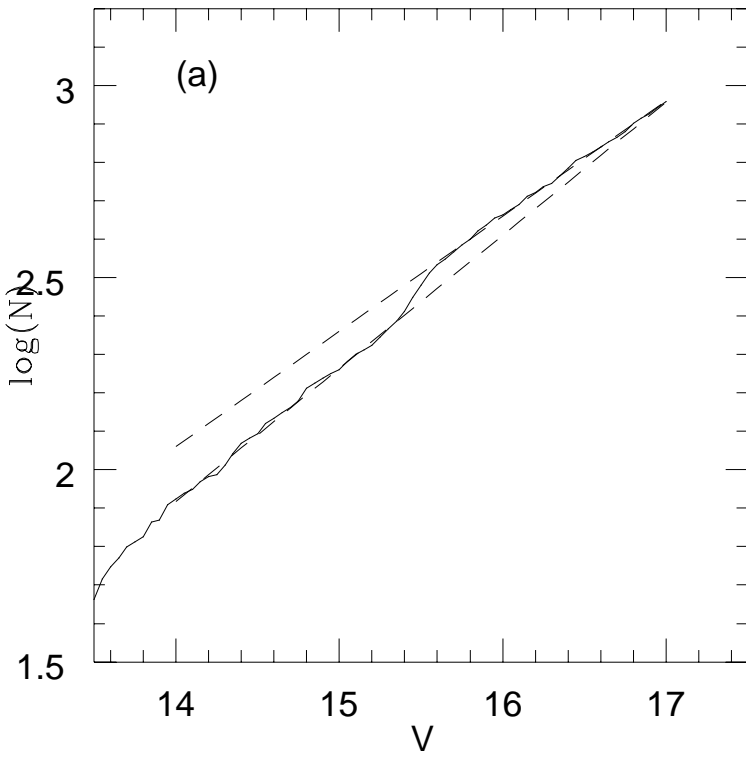


This figure "5478f15.gif" is available in "gif" format from:

<http://arxiv.org/ps/astro-ph/9611016v1>

This figure "5478f16.gif" is available in "gif" format from:

<http://arxiv.org/ps/astro-ph/9611016v1>



This figure "5478f18.gif" is available in "gif" format from:

<http://arxiv.org/ps/astro-ph/9611016v1>

This figure "5478f19.gif" is available in "gif" format from:

<http://arxiv.org/ps/astro-ph/9611016v1>